Examensarbete vid Institutionen för geovetenskaper
ISSN 1650-6553 Nr 125

Statistical Characteristics of Convective Storms in Darwin, Northern Australia

Andreas Vallgren

Abstract

This M. Sc. thesis studies the statistical characteristics of convective storms in a monsoon regime in Darwin, northern Australia. It has been conducted with the use of radar. Enhanced knowledge of tropical convection is essential in studies of the global climate, and this study aims to bring light on some special characteristics of storms in a tropical environment. The observed behaviour of convective storms can be implemented in the parameterisation of these in cloud-resolving regional and global models. The wet season was subdivided into three regimes; build-up and breaks, the monsoon and the dry monsoon. Using a cell tracking system called TITAN, these regimes were shown to support different storm characteristics in terms of their temporal, spatial and height distributions. The build-up and break storms were seen to be more vigorous and particularly modulated diurnally by sea breezes. The monsoon was dominated by frequent but less intense and vertically less extensive convective cores. The explanation for this could be found in the atmospheric environment, with monsoonal convection having oceanic origins together with a mean upward motion of air through the depth of the troposphere. The dry monsoon was characterised by suppressed convection due to the presence of dry mid-level air. The effects of wind shear on convective line orientations were examined. The results show a diurnal evolution from low-level shear parallel orientations of convective lines to low-level shear perpendicular during build-up and breaks. The monsoon was dominated by complex orientations of convective lines.

The thesis includes a study of merged and splitted cells, which have been separated from other storms, and mergers were shown to support more vigorous convection in terms of height distribution and reflectivity profiles. They were also seen to be the most long-lived category of storms as well as the most common type. Split storms were generally weaker, indicative of their general tendency to decay shortly after the split occurred.

Sammanfattning

En statistisk studie av konvektiva celler i en miljö som präglas av monsunförhållanden har utförts i Darwin, norra Australien, med hjälp av radar.
En ökad förståelse för tropisk konvektion är nödvändig för att kunna studera klimatet globalt. Denna studie har bidragit till denna kunskapsbas genom att studera några viktiga parametrar hos konvektiva celler i en tropisk miljö. De observerade egenskaperna hos dessa celler kan implementeras i parametriseringen av högupplösta regionala och globala modeller. Regnperioden delades upp i tre olika regimer; uppbyggnad och avbrott, monsun och torr monsun. Genom att använda ett cellsökande system kallat TITAN, visade sig dessa regimer uppvisa olika karakteristika vad gäller tids- och rumsmässig samt vertikal distribution av konvektionsceller. Uppbyggnad- och avbrottsregimen dominerades av mäktiga och intensiva konvektionsceller, och modulerades av sjöbrisar på en daglig basis. Monsunen dominerades av talrika men mindre intensiva celler. Anledningen till detta kan finnas i atmosfäriska förhållanden, där monsunen dominerades av konvektionsceller med oceanisk härkomst och allmän hävning genom större delen av troposfären. Den torra monsunen präglades av försvagad konvektion på grund av närvaron av mycket torr luft på medelhöga nivåer. Effekten av vindskjuvning på orienteringen av bylinjer undersöktes. Resultaten visar att en daglig övergång från en orientering som var parallell med vindskjuvningsvektorn till en vinkelrät orientering dominerade under uppbyggnad och avbrott. Monsunen präglades av komplexa orienteringar av bylinjer.

Sammanväxande och splittrande celler separerades från andra celler och undersöktes speciellt. De sammanväxande cellerna uppvisade mer intensiv konvektion och större vertikal mäktighet. Denna kategori av celler, som var den vanligaste typen av icke-isolerade celler, levde också längre än andra celltyper. Splittrande celler var generellt svagare än andra celler, vilket indikerade den generella tendensen för denna celltyp att brytas ner strax efter det att en splittring ägt rum.

Preface

Ever since I left Australia in 2004 after having spent six months as an exchange student at Monash University in Melbourne, I tried to find ways of coming back for another stay. My earlier professor Nigel Tapper at Monash University suggested me to come back for a cloud experiment that was about to take place in 2006. I came in touch with Steve Siems at the department of Mathematical Sciences, Monash University. He directed me to Peter May and Christian Jakob at the Bureau of Meteorology Research Centre (BMRC) in Melbourne. This was the beginning of what was to come. After three years of intense studies at Luleå University of Technology, and another two years at Uppsala University, I left Sweden for Australia on October 31, 2005. The following six months were devoted to hard work in the field of tropical meteorology.

After two months of preparatory work at the BMRC in Melbourne, I left for Darwin in January 2006, in order to participate in one of the largest meteorological experiments in recent years: the Tropical Warm Pool – International Cloud Experiment (TWP-ICE). It was one beautiful month in my life, where I met many new friends and colleagues with one thing in common: a passion for tropical weather! This passion manifested itself in long days of work followed by nice dinners in the warm tropical evenings at the Darwin harbour, watching the lightning strikes from the powerful storms over the continent.

I would like to thank many people for their helpfulness during my stay in Australia. First, I would like to thank my supervisor Peter May, BMRC, without whom none of these studies would have been possible. Thanks also to Kevin Cheong for help in accessing all the TITAN data, and to Michael Whimpey and Alan Seed for recreating radar data on request at any time. Courtney Schumacher, Texas A&M University, has encouraged and motivated me, not only during the field experiment, but also afterwards. Thanks also to Ed Zipser, University of Utah, who gave me valuable suggestions on things to look at in the overwhelming dataset. Thanks Christian Jakob, BMRC, for giving me feedback on my final presentation in Australia and for your always happy smile! A great thank you also to my examiners Sven Israelsson and Ann-Sofi Smedman, Uppsala University, who helped me with home issues and carefully read through this thesis and came with valuable suggestions. Thanks also to Salomon Eliasson, my student colleague from Uppsala in Melbourne for all fruitful discussions. Finally, I would like to acknowledge my close friend Johan Liakka. Your support has been, and will always be, invaluable!

The contents of this thesis will be presented at the Nordic Meteorology Meeting in Uppsala in September 2006 together with a poster. Furthermore, an article will be written on the basis of the findings in this diploma work, together with my supervisor Peter May.

Andreas Vallgren
Uppsala, May 2006

CONTENTS

Chapter 1

Introduction

The summer in tropical northern Australia is characterised by warm and wet conditions. The rain comes as convective showers and thunderstorms, often in association with propagating squall-lines (e.g., Riehl, 1954; Tapper, 1996; Keenan and Carbone, 1992; Drosdowsky, 1996). Since the Sun is the driver of Earth's climate system, the deep convection occurring in the Tropics, including tropical northern Australia, constitutes the major heat source in the global climate (Houze and Mapes, 1992). In order to understand and correctly parameterise the fluxes of heat and moisture, it is essential to understand the weather and climate of these regions.

Since rain in the Tropics falls from convective clouds, these are of particular importance. However, convective clouds do not behave as an entity. They appear in a wide variety of shapes and under very different atmospheric conditions. The aim of this study is to assess and quantify the behaviour of these convective clouds when they are extensive enough to cause convective rainfall. By radar retrievals from a radar station outside Darwin, the statistical behaviour of storms under different conditions can be quantified. One of the largest field programs in meteorology in recent years was held in Darwin in the beginning of 2006; Tropical Warm Pool – International Cloud Experiment (TWP-ICE). This thesis has been performed in association with the experiment.

Ballinger and May (2006) studied the statistical characteristics of convective storm height, size and duration during the wet season of 2003/04. This study will focus on additional aspects of convection in the region, such as the storm orientations with respect to vertical wind shear under different convective regimes as well as the height distribution of subsets of storms that have been described only in terms of case studies before (e.g., Keenan and Carbone, 1992; Wilson et al., 2000). Furthermore, the reflectivity profiles, cell lifetimes and cell speeds with respect to the steering flow will be addressed and quantitatively compared between different regimes. Another aim is to study the behaviour of mergers and splits as compared to isolated cells. Knowledge about these statistical characteristics will improve the understanding of the behaviour of convection in northern Australia, which can improve the parameterisation of convective storms in weather forecast- and cloud-resolving climate models. Furthermore, the observations might be used to make short-range forecasts and can be applied to other monsoonal regimes of the world.

Darwin is a very good location for such studies since the weather is characterised by a great degree of variability. Furthermore, the radar station covers continental, oceanic and island regions, all having their very own special environment. However, in order to conduct the study optimally, we need to know something about the weather and climate of northern Australia and how radars work. Therefore, the next chapter gives a background to the relevant theory.

Chapter 2

Theory

The northern part of the Australian continent is situated in close proximity to the equator and the Arafura and Timor seas, which influences the weather and climate of the region. It is under the influence of large-scale circulations such as the Hadley cell, which are fundamental in the global atmospheric circulation. The centre of the continent is semi-arid to arid and therefore gives rise to a very dry continental air-mass, as opposed to the moist air masses found over the adjacent oceans. The incoming solar radiation heats the surface, which, in turn, warms the air closest to the surface, becoming less dense. Climatologically, this is seen in the presence of a mean surface trough in the equatorial region. The orientation of this trough strongly depends on the surface characteristics including the distribution of land and ocean. It is also seen to follow the motion of the Sun so that we find the trough mostly on the summer side of the planet. During the winter of the southern hemisphere, the near-equatorial trough (also referred to as the Inter Tropical Convergence Zone, ITCZ) is located well north of the Australian continent, which is dominated by eastward-moving anticyclones that slow and intensify over the interior of the continent due to the cooling of the surface at this time of year (Ramage, 1971). The weather is therefore quasi-stationary, with a steady wind from southeast (the trade winds) and an abundance of sunshine. These conditions persist throughout the winter, giving rise to very dry conditions.

During spring, the continent heats up, causing the mean surface anticyclone over the continent to be replaced by an extensive heat-low. Sunny weather is maintained in the heat-low region through upper tropospheric convergence, which gives rise to descending motions and associated cloud dissipation. The establishment of an extensive permanent heat-low initiates a steady inflow of moist maritime air, which can be seen as a large-scale sea breeze, as pictured in figure 2-1. The continent at this time of year is characterised by an increasingly hot and dry air mass. Dew points are near 0^{o}C inland, which causes a moisture discontinuity to develop on the boundary to the moist air of oceanic origins with dew points above 20^{o}C (Tapper, 1996). If no synoptic scale disturbances are present, a steady state situation results where the air mixes. Together with stable conditions at the 700 hPa level, convection is inhibited and the heat trough can persist, as the lack of clouds supports the continuation of solar heating.

However, the heat trough is dynamic, and as such, it responds to different triggering mechanisms, described by Tapper (1996). One such mechanism is the equator-ward progression of mid-latitude cold fronts into the heat trough from the far south, on the eastern flank of eastward progressing anticyclones. These cold fronts, who have lost most of their original characteristics, help to push the trough northward, causing low-level convergence in the moist air north of the trough and convection can initiate.

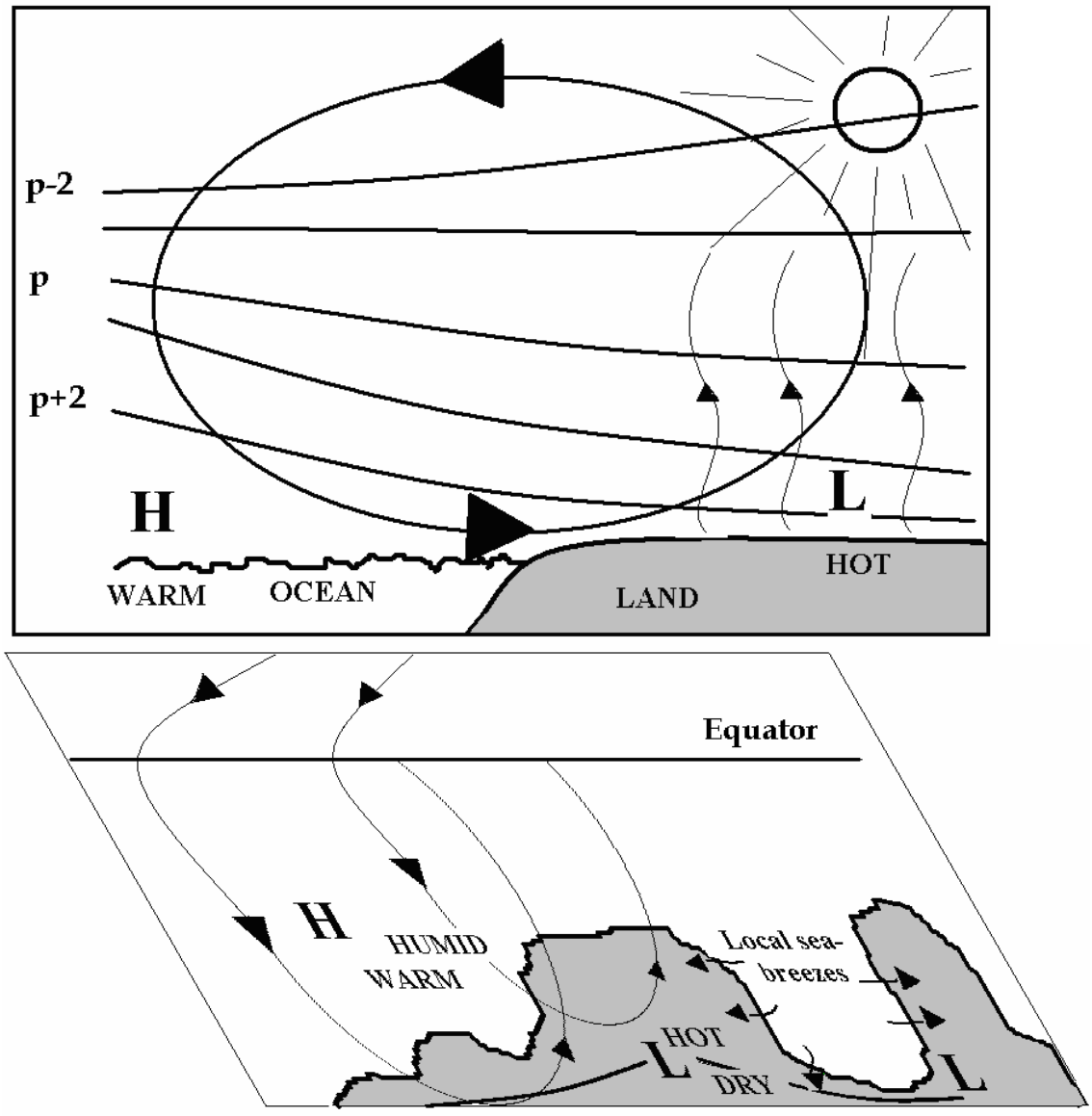

Fig. 2-1. A conceptual model of the circulation system over northern Australia in summer. The topmost figure represents the initiation of a sea breeze due to the diurnal heating of land surfaces. The isobars (constant pressure) are indicated through an atmospheric column. The bottom figure shows the result of large-scale heating on the development of a monsoon circulation. The semi-persistent heat-trough is indicated, as well as the deflection of air currents due to the Coriolis effect.

Anticyclones over southern Australia can also trigger disturbances on the trough line due to horizontal wind shear. Another synoptic scale mechanism that can help to initiate convection is the equator-ward extension of a long wave trough (mid-latitude Rossby wave) in the upper troposphere. If this is superimposed on a surface heat-low, it induces a mean vertical ascent of air, which gives rise to low-level convergence, destabilising the mid-troposphere, which facilitates convection.

North of the heat trough, the *monsoon* prevails. Ramage (1971) has defined a monsoon regime to be present if the prevailing wind direction shifts by at least 120^{o} between January and July and the average frequency of prevailing wind directions in January and July exceeds 40%. Furthermore the mean resultant wind at least one of

the months should exceed 3 ms^{-1}. The monsoon blows in response to the seasonal change that occurs in the pressure gradient resulting from the differences in temperature between land and ocean. It is characterized by warm and moist westerlies through a depth of the atmosphere up to about 400 hPa with easterlies aloft (Tapper, 1996). The low-level westerlies originate in the northern hemisphere, even though the cross-equatorial flow is limited due to a weak pressure gradient near Indonesia. The westerlies reach about 15°S over the Australian continent. They are strongest in the west where the land-sea temperature gradients are the greatest (Ramage, 1971). The mean onset date of the monsoon in northern Australia is the 28th of December and the mean retreat occurs 75 days later, on March 13, but the interannual variability is considerable (Drosdowsky, 1996). The monsoon is characterised by bursts of westerlies in the low levels associated with abundant rainfall, and drier break periods, when the zonal wind in the low levels weakens and can turn back into easterlies. In both regimes, the weather is governed by convection. Moist convection generates the rain bearing tropical clouds and some important parameters in studies of convection will be introduced in section 2.2. First, a brief overview of the variability of climate will be outlined.

2.1 Variability in climate

The interannual and intraseasonal variability of rainfall in the very north of Australia is substantial. Disturbances of interest are, for example, tropical depressions and tropical cyclones. These systems tend to develop in the vicinity of the monsoon trough and can strongly influence the monsoon circulation and also the onset/breaks of the monsoon. Every year, a number of tropical cyclones appear near the Top End and can bring extreme rainfalls. Drosdowsky (1996) concluded that a substantial portion of the annual rainfall is caused by tropical cyclones and squall-lines moving in strong easterly flows pole-ward of the monsoon trough.

Some particular large-scale influences on observed weather and climate deserve some attention. The El Niño Southern Oscillation (ENSO) is a well-known feature of the Australian climate. The ENSO is associated with abnormal sea levels and sea surface temperatures across the Pacific and acts to shift the location of most favourable convection from the maritime continent north of Australia towards Latin America during the famous El Niño phase. This might influence the time of onset of the monsoon, being delayed by a present El Niño, whereas early onsets tend to precede El Niños (Tapper, 1996).

A more important factor in the climate variability for northern Australia might be the so-called Madden-Julian oscillation (MJO), or 40-50 days oscillation, as it is also referred to in the literature (McBride and Frank, 2005). Madden-Julian (1994) describes the oscillation as a result of large-scale circulation cells oriented in the equatorial plane that move eastward, causing anomalies in the zonal wind and divergence in the upper troposphere, which has an effect on the convective activity through its influence on static stability. These waves often travel eastward around

the circumference of the globe. The effect of these can be seen in the progression of regions of enhanced convection. For northern Australia, the effects are seen mainly in the timing of the onset of the monsoon. On average, it takes about 40 days between the active bursts of the monsoon. The MJO explains about 40% of the variability in rainfall (McBride and Wheeler, 2005). Another important aspect of the MJO is that it causes a pole-ward expansion of convective activity, bringing essential rainfalls to the semi-arid areas further south. McBride and Wheeler (2005) outline some other features of importance, such as the convective-coupled Kelvin and internal equatorial Rossby waves, which act to enhance convection under certain circumstances. Some parameters which are important in convection will now be described.

2.2 Some important aspects of convection

Two important parameters that can be calculated from an aerological diagram and that will be used in the analysis in chapter 3, are CAPE (Convective Available Potential Energy) and CIN (Convective Inhibition) defined as follows (in J kg^{-1}):

$$CAPE = g \int_{LFC}^{Z_T} \frac{\theta(z) - \bar{\theta}(z)}{\bar{\theta}(z)} dz \,, \tag{2.1}$$

$$CIN = -g \int_{Z_0}^{LFC} \frac{\theta(z) - \bar{\theta}(z)}{\bar{\theta}(z)} dz \,. \tag{2.2}$$

In these equations, θ is the potential temperature of an air parcel and $\bar{\theta}$ is the environmental potential temperature through the atmosphere. LFC is the level of free convection, i.e., where an air parcel becomes warmer than the environment, whereas Z_0 is the ground level, and Z_T is the approximate cloud top (assumed to be where $\theta = \bar{\theta}$). CIN is simply the negative counterpart to CAPE, since it gives an indication of the energy an air parcel need to gain before the conditional instability can be released, i.e., for an air parcel to reach the level of condensation. It reflects the strength of capping inversions, and needs to be overcome if convection should continue, since the air parcel is cooler than its environment in a layer of positive CIN. CAPE and CIN can be calculated from a thermodynamic diagram as the area between the parcel and the environmental temperature, if the scales are adjusted so that the area is proportional to energy (Houze, 1993). CAPE gives an indication of the amount of potential energy that can be transformed into kinetic energy, which determines the maximum possible magnitude of the updrafts. From the vertical momentum equation, the maximum vertical wind can be found to be proportional to $\sqrt{CAPE}$. The strength of updrafts will be seen to be important in generation of precipitation.

If no lifting mechanisms are present, and the CIN cannot be overcome, the CAPE can continue to build-up without being released. Therefore, the highest CAPE conditions are actually found in cloud-free areas of the Tropics. It is noteworthy that air parcels

raised from above 900 hPa rarely become positively buoyant in the Tropics as implied by soundings, and tropical convective clouds therefore tend to have low cloud bases during their build-up (McBride and Frank, 1999). Consequently, CAPE is sensitive to boundary layer variations in temperature and moisture. The combination of temperature and moisture can be represented by the equivalent potential temperature, θ_e (derived in appendix A). This temperature can be used to compare both the temperature and moisture content of different air masses. θ_e gives an indication of the latent heat content of air, which is important in sustaining convective updrafts. The higher the θ_e, the more heat and/or moisture content of the air. The profiles of θ_e under two important regimes are given in figure 2-2.

Another important aspect of convective characteristics is the moderating effect of entrainment, i.e., environmental air crossing the cloud boundaries and mixing with the saturated air. Houze (1993) points out that entrainment of environmental air occurs as a result of the highly turbulent motions in convective cells. The entrainment occurs at all edges of the cloud. The drop size spectrum, total water content and cloud height are all affected by entrainment (Houze, 1993). Rogers and Yau (1989) suggest that the moderating effect of entrainment on convective intensity is that of mixing cooler and drier air from the surroundings with the warmer and moister buoyant air. The opposite effect to entrainment is detrainment, which describes the process of diluting air from a convective current to its surroundings. This effect acts to drain the convective core on some of its content, making the convection less vigorous.

It is worthwhile to look at some characteristics of cloud generation. In the Tropics, there are four major factors that control vertical motions and possible subsequent cloud growth (Riehl, 1954). These are the horizontal convergence in the wind field, the mean depth of the moist layer, the vertical stability and lifting due to orography. May and Rajopadhyaya (1999) found that the most intense updrafts occurred above the freezing level, but that also shallow convection can show large vertical velocities. However, they conclude that the magnitude of vertical velocities observed in tropical convection cells are less than for intense mid-latitude convection. This stems to the observation that CAPE is distributed over a deeper layer than their mid-latitude counterparts. The height distribution of CAPE is a limiting factor in the maximum achievable magnitudes of updrafts. Monsoon storms show more uniform profiles of updrafts as opposed to the break storms, which have a double peak in the profiles (May and Rajopadhyaya, 1999). The lower peak is associated with warm rain and glaciation whereas the upper peak is associated with a decrease in precipitation loading. Now, the mesoscale characteristics of convection in northern Australia will be outlined.

2.3 Mesoscale characteristics of the northern Australian wet season

Most convective cells are relatively weak, isolated and short-lived, but at times they are intense, organised and long-lived. They appear in a broad spectrum of situations

ranging from diurnal isolated cells to lines of enhanced convection, squall-lines, mesoscale convective systems (MCSs) into impressive tropical cyclones. Dynamic features that favour and control the development and maintenance of convection range from sea breeze convergence lines to upper-level vorticity, wind shear and cold pool propagation (Mapes and Houze, 1992; Keenan and Carbone, 1992; Wilson et al., 2000; Hamilton et al., 2004). Although convection might be the driver behind almost all tropical rainfall, there is still a contribution to the total rainfall from stratiform rain. However, stratiform rain has convective origins in the Tropics rather than from large-scale ascent as seen in mid-latitude systems. In MCSs, only about 10% of the system is characterised by convective activity and the remainder is dominated by stratiform rain (Houze, 1993). The stratiform region, originating from early convective activity, is dictated by weaker vertical winds (Houze, 1997). The following will describe the dynamics behind rainfall in the region during the different regimes, i.e., build-up, breaks and the monsoon. The build-up is defined as the period preceding the arrival of the monsoonal westerlies. The breaks are characterised by an equator-ward movement of the monsoon trough to the north of the continent. They are often preceded by sudden and dramatic dryings that extend through the depth of the atmosphere, caused by horizontal dry air advection (McBride and Frank, 1999). The next section will introduce the characteristics of convection occurring during the build-up and break periods.

2.3.1 Build-up and break convection

The build-up and breaks are dominated by a strong diurnal modulation of convective activity in a generally conditionally unstable tropospheric stratification. Studies (e.g. McBride and Frank, 1999; Keenan and Carbone, 1992) have shown that the lower troposphere is slightly but consistently warmer during build-up and breaks than the monsoon, whereas the upper levels are slightly cooler, which causes a destabilisation of the troposphere. The same studies have shown that CAPE is inversely related to convective activity, but that variations in CAPE are related to the severity of the convective storms once they form. The initiation mechanisms behind convection will be described in section 2.3.3. First, the monsoon characteristics will be described.

2.3.2 Monsoonal convection

The conditions during the active phases of the monsoon support abundant, but less intense, convection than during inactive phases. The active monsoon is characterised by a pole-ward extending monsoon trough, strong low-level westerlies and upper-level easterlies. Keenan and Carbone (1992) found that the monsoon differs in terms of the extreme vertical development seen in build-up and break storms with their general lack of stratiform decks (other than those associated with squall-lines). Substantial rainfall and relatively intense echoes are found also in a monsoon regime, but these are generally confined to lower altitudes, mostly below the melting level.

The monsoon is a large-scale phenomenon with spatially extensive regions of precipitation, as compared to the localised convection during build-up and breaks.

Houze and Mapes (1992) hypothesised that the monsoon is an unstable positive-feedback process, in which deep convection, once triggered, favours additional deep convection. They concluded that localised convective heating in the troposphere spins up both mesoscale vortices, as well as the large-scale monsoon circulation. Despite observations of a warmer upper troposphere during monsoonal conditions, implying less buoyancy and CAPE, convective activity did not decrease with time. This suggests that low-level processes are dominating the observed monsoon characteristics. The low-level processes found to support the circulation and maintain the convective activity are mostly positive feedback processes. These include evaporation enhancement by convectively induced surface winds, humidification of the dry atmosphere by convection and boundary layer cold pool propagation (Houze and Mapes, 1992). It should be kept in mind that although the boundary layer air tend to be cooler during monsoonal conditions, the higher moisture content conserves the equivalent potential temperature, important in the release of CAPE. Furthermore, convectively disturbed boundary layer air has been observed to restore into a state of convective readiness within half a day through surface fluxes (Houze and Mapes, 1992). This implies that active monsoon periods are not limited by earlier convective overturning. The abundant convection is often found in relatively large mesoscale convective systems with large stratiform regions.

The more favourable conditions for convection to occur during the monsoon can be understood from figure 2-2, showing the profiles of potential and equivalent potential temperatures during the 2005/06 wet season. It is evident that the monsoon shows slightly cooler potential temperatures than build-up and breaks but a higher equivalent potential temperature, indicating a large content of moisture (latent heat), especially in the middle and upper troposphere. The build-up and breaks show larger equivalent potential temperatures than the monsoon in the lowest layers, and the effects of this will be discussed in the analysis in chapter 3.

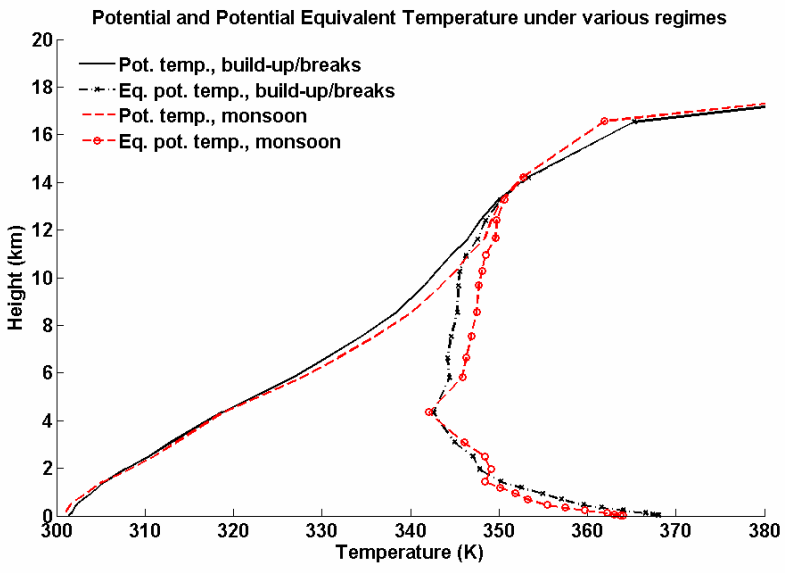

Figure 2-2. Profiles of potential and equivalent potential temperatures from TXLAPS diagnosis 2005/06. The equivalent potential temperature gives a combined measure of moisture and heat content of air with height. The temperature measures have been separated into the different regimes, i.e., build-up/breaks and the monsoon. The x-axis gives the temperature in K, whereas the y-axis shows the geopotential height above ground in km.

Now, the convective initiation mechanisms required during the build-up and breaks will be introduced, starting with the primary driver; sea breezes. Then the results, such as formation of squall-lines and trailing stratiform precipitation, influence of wind shear and effects of merging of cells will be outlined.

2.3.3 Sea breeze initiation of convection

The Tiwi islands (Bathurst and Melville island) north of Darwin constitute a unique atmospheric laboratory, in which many important aspects of convection can be studied. The Tiwi islands are, seen as a unity, approximately elliptical and zonally oriented at 11 ^{o}S, with a zonal extension of nearly 150 km and meridionally ~50 km. A 1-7 km wide strait separates the islands, which are nearly flat, with a 120 m maximum elevation. The following discussion is based on studies pursued during the Maritime Continent Thunderstorm Experiment (MCTEX) 1995. Thunderstorms occur at ~65% of the days during the build-up and break periods over the Tiwi islands (Keenan and Carbone, 1992). Their frequent presence has given them their own name; *Hectors*. These will be defined as storms occurring over the Tiwi islands at daytime (11.30 – 18.30 LT) during build-up and breaks. Wilson et al. (2000) studied diurnally forced convection over the Tiwi islands and found that all convective storms could be traced back to early sea breezes. This is the case also for the coastal regions of northern Australia. A complex interaction of sea breezes, propagating cold pools (i.e., areas of cooler air formed by evaporative cooling in convective downdrafts) and low level shear were seen to play a major role in the organisation of mature convective systems. Wilson et al. (2000) suggest a multiple-stage forcing process including up to five mechanisms to be responsible for most of the storms (~80%) occurring over the Tiwi islands, and will now be briefly explained.

Solar heating during the morning initiates a well-developed sea breeze circulation along the coasts as the boundary layer is growing and a density discontinuity develops, along which convection initiates and clouds form. Subcloud evaporation of raindrops cools the air and generates downdrafts and convectively driven cold pools. These cold pools are shown to introduce a chain reaction of localised convergence zones (Wilson et al., 2000). Radially spreading cold pools force air to rise, causing new cell developments, which, in turn, create cold pools on their own. This causes a quasi-chaotic picture in what was once the undisturbed boundary layer further inland. This is an essential stage for further development, detached from the orderly behaviour of the sea breeze circulations along the coasts. It frees the convection from the sea breeze fronts and causes self-organised and self-sustained travelling storms.

Moncrieff and Liu (1999) point out that the commonly used hypothesis that initiation of a sea breeze is strongly suppressed on the windward coast and enhanced at the leeward side is true only if shear and surface flow have opposite signs. Given that sea breezes are quasi-normal to the coastlines, and a quasi-easterly wind at 700 hPa, the shear-vector will point in a generally westward direction at all times in the low levels during build-up and breaks. This would favour an apparent westerly

propagation for the bulk of the cells. Moncrieff and Liu (1999) conclude that downshear propagating outflows, having a speed equivalent to that of the steering level, show overturning updrafts that provide deep lifting, which is fundamental in dynamical organisation of the convection. The organisation of these cells has been shown to evolve from nearly shear-parallel towards an orientation perpendicular to the low level shear-vector. This is the case both for the Tiwi islands and the continental regions (Keenan and Carbone, 1992) due to the dominance of zonally oriented sea breeze fronts. The observed organisation has to do with the characteristics of the flow above the boundary layer, which during build-up and break season is dominated by dry easterlies. A rear inflow of dry air into an erect convective current (entrainment) causes evaporation and cooling. This induces a downdraft at the rear side, enhancing the development of a spreading cold pool, which was found to favour downshear convection. Wilson et al. (2000) suggest that in the case of Tiwi islands convection, reorientation can occur also because of vigorous or colliding gust fronts from separate convective areas over Bathurst and Melville islands. Colliding gust fronts have been found to yield the most intense convective systems. These can in extreme cases generate updrafts as strong as 40 ms^{-1} (Hamilton et al., 2004).

During suppressed conditions, another more direct type of mechanism can cause convection, but often at a later time of the day. This type is caused by direct collision of inward propagating sea breezes. The tendency for new cell growth to occur at the western boundary of a cold pool, favours the formation of meridional convective lines, i.e., squall-lines. Squall-lines are important rain-bearing features of the Top End during the build-up and break periods and will now be introduced.

2.3.4 Squall-lines

Squall-lines are defined as non-frontal lines of active convective storms, which exist for a considerably longer time scale than the lifetime of the individual cumulonimbus cells, making up the squall-line (Ramage, 1971). These systems have the ability to persist overnight when other convection has weakened. Wind shear is important in sustaining the squall-lines as has been found for Darwin cases (e.g. Keenan and Carbone, 1992). A common type of squall-line in northern Australia is the one which has trailing stratiform precipitation. Figure 2-3 (from Houze, 1993) represents a model of this type of squall-line. The front side of the squall-line is characterised by an upward motion that begins in the boundary layer with high equivalent potential temperatures extending up into the convective region. The continuity of the system is maintained by an associated downward motion of air from the mid-levels into the rear of the squall-line, which extends down to the low-levels, contributing to the spreading gust front. The presence of dry air causes enhanced evaporative cooling and the development of a cold pool. Superimposed on the general up-flow region are areas of intense localised updrafts and downdrafts. As new cells form, the old ones are advected rearwards over the layer of dense subsiding inflow from the rear. The dynamics of these will now be briefly explained.

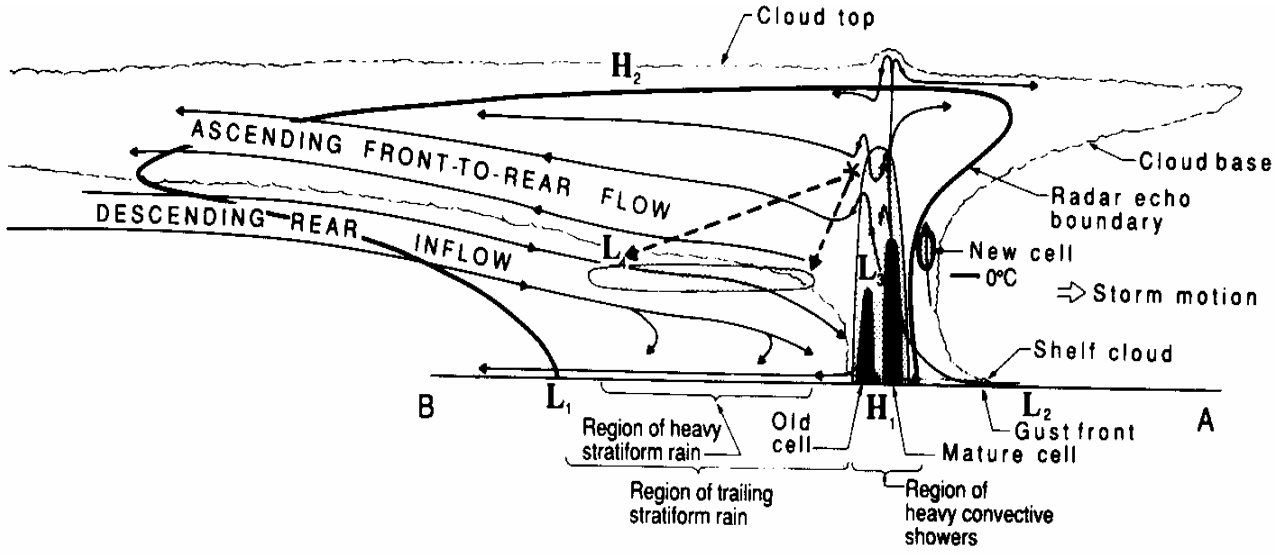

Figure 2-3. Conceptual model of a squall-line with a trailing stratiform region. From Houze (1993). The right side represents the frontside of the squall-line. Characteristic shelf clouds might precede the squall-line along with a gust and vertically extensive cumulonimbus clouds. The most intense cells are found on the front, followed by a region of weaker cells and stratiform precipitation. The updrafts found close to the front are replaced by slowly descending air at low levels as the squall-line passes whereas a weak upflow is evident above the mid-levels.

2.3.5 Stratiform regions following a squall-line

In regions of older convection, the vertical motions are weaker, and the precipitation particles falls slowly, gaining mass through vapour diffusion (Houze, 1997). This induces a three-layered response, where environmental air converges at midlevels with associated divergence below and above this region (Houze, 1997). This can be compared to the two-layered response in the convectively active regions with low level convergence and upper level divergence. Stratiform precipitation can be defined by a particular set of microphysical processes leading to the fallout of precipitation in a regime of wide horizontal weak upward motion. In radar observations, this can be seen as thin and horizontally extensive regions of rather uniform echoes, instead of the vertically extensive cores of intense echoes generally seen in convective regions. An important implication from dynamical reasoning is that new convection is encouraged in the immediate surroundings of a region dominated by stratiform rain. The influence of wind shear on convective organisation into squall-lines will now be outlined.

2.3.6 Influence of vertical wind shear on convective organisation

Different shear regimes have been shown to influence the organisation of cells in a wide variety of ways. LeMone et al. (1998) studied the organisation of mesoscale convective systems over the western Pacific in TOGA-COARE 1992-1993 and their findings will now be discussed.

The structure of an MCS can be determined by environmental wind, temperature and humidity profiles. This behaviour of MCSs is referred to as 'self-organisation', which has been shown to be important in organising convection in the Tropics. LeMone et al. (1998) sorted the convective organisation into five categories. Lines nearly perpendicular to the low-level shear were in TOGA-COARE found to form during low-level shear conditions in excess of 2 m s^{-1} per 100 hPa in the lowest layers, and they were dominated by mass fluxes into the lines from the front. Shear-parallell lines on the other hand, tended to be parallel with the shear at midlevels, between 800 and 400 hPa, in cases when midlevel shear dominated over low-level shear and this shear exceeded 5 ms^{-1}. These bands remained stationary (although with overall short lifetimes), whereas the individual cells propagated in discrete jumps. Smaller-scale convection forming lines was often relatively shallow and modulated by different mechanisms such as gravity waves and cold pools which complicated the analysis.

LeMone et al. (1998) also found that if both low- and mid-level shear are strong, the primary band will be shear-perpendicular, and the midlevel shear will determine the presence of secondary bands. If the mid-level shear has a significant rearward component, secondary bands parallel to the midlevel shear form behind the primary band about 3-4 hours after the development of a primary band.

In situations with widespread convection, the discussion above is complicated due to interactions between cold pools and gravity waves. The formation of convective lines is based on the fundamental process of merging of cells.

2.3.7 Mergers and splits

Studies have shown that clouds where cells have merged (≡ mergers) are larger and produce more rain than the sum of isolated systems (Westscott, 1994). Common merging mechanisms are bridging between cells of different ages and sizes, low-level convergence in association with strong shear, differential cell motion and horizontal expansion of echo cores (Westscott, 1994). Westscott (1994) showed that the subset of cells that were growing before a merge occurred continued to do so after the actual merge, and that a large fraction of these cells increased in area, height or reflectivity before the merge. Merging is a passive process but is often an indication of the presence of active and organised convection, causing mergers to show more vigorous and intense updrafts and taller sizes than non-mergers (Westscott, 1994). Simpson et al. (1993) showed that about 90% of the total rainfall over the Tiwi Islands come from merged systems, although these comprise only about 10% of the convective systems. It is common that first order merging occurs along local sea breeze convergence lines. The development of a cold pool then enhances the merging of cells along the downshear flank of the complex. The complexity of convection makes rainfall highly variable in space and time. The use of radar technology to study and quantify the behaviour of convective cells will now be introduced.

2.4 Data and methodology

This section describes the microphysical and statistical characteristics of precipitating systems in terms of radar observations, and the data collected in this study. First, an introduction to radar theory will be presented.

2.4.1 Radar theory

Radar systems are an integral part of research studies because of its ability to study rain over large areas. A radar emits short pulses of electromagnetic waves that illuminate the meteorological objects of interest. An automatic switch changes the mode between a transmitting and a receiving mode, during which the antenna collects the reflected radiation. Many meteorological radars operate in the spectral region of 1-10 cm wavelength. The scattering and absorption of atmospheric gases and small particles are very low in this region as compared to that by precipitating hydrometeors, e.g. rain/snow (Karlsson, 1997). The physics behind the technology can be formulated by the following, commonly used, approximate radar equation (Anderson et al., 1985):

$$\Pr = \frac{C \cdot |K|^2 \cdot Z}{r^2} \cdot 10^{-0.2\int k \cdot dr} \tag{2.3}$$

It shows the parameters of greatest importance in meteorological terms. Pr is the effect of the return signal as an average for many pulses, C is a constant dependent on the apparatus in use, $|K|^2$ = 0.93 for water and 0.20 for ice where K is the refractive index, r is the distance between the antenna and the reflecting object, whereas Z is the reflectivity factor, which will be further examined shortly. The term $10^{-0.2\int k \cdot dr}$ gives the damping caused by gases, in particular hydrometeors of the atmosphere (Anderson et al., 1985). An important assumption is that the meteorological objects are much smaller than the wavelength of the beam, and that they are isotropically distributed in the pulse volume. The radar equation is usually presented in its logarithmic form, giving values in decibel (dB), with 0.001 W as a reference value. The common form of the reflectivity factor is $10 \cdot \log(Z) \equiv$ dBz, giving:

$$\Pr(dB) = C_1 + 10 \cdot \log|K|^2 + dBz - 20 \cdot \log(r) - 2 \cdot \int k \cdot dr \tag{2.4}$$

The reflectivity factor Z is defined as $Z \equiv \frac{1}{\Delta V} \sum_i D_i^6$ where ΔV is the pulse volume, D is the diameter of a droplet (in mm) and Z is given in $mm^6\ m^{-3}$. It is clear that the drop-size is of fundamental importance in the return signal to the radar. The information of interest is to relate the return signal to precipitation intensities. Assuming that all of the detected particles precipitate, then using an empirical drop size distribution such as the Marshall-Palmer raindrop size distribution, leads to a relationship between reflectivity and precipitation intensity (Karlsson, 1997). The relationship varies with intensity of rainfall and type of hydrometeors. Comparing

radar echoes with actual rain gauges at a specific location for a long period of time makes it possible to derive an empirical Z-R relationship of good use. However, other complications occur when hydrometeors, such as hail, occur in a storm. This is particularly the case if the hailstones are large and wet, which could cause Mie scattering rather than Rayleigh scattering to dominate. This violates the assumption of small hydrometeors compared to the wavelength (Karlsson, 1997). Another effect that can be seen is when snowflakes, mostly in stratiform precipitation, start to melt, creating a thin layer of water surrounding the snowflake, which can give rise to high reflectivity values that peak out just below the 0 ^{o}C region. This phenomenon is called the bright-band effect. Table 2-1 relates the intensity of rainfall to corresponding dBz-values in order to simplify the discussion in subsequent chapters.

Table 2-1. Approximate relation between reflectivity and rain rate. (Doviak & Zrnic,1993; Rogers & Yau, 1989).

Reflectivity (dBz)	**Rainfall rate (mm h^{-1})**	**Intensity**
< 15	≤ 0.3	Trace to very light
25	~ 1	Light
35	~5	Moderate
45	~25	Moderate to heavy
55	~100	Very heavy, possibly hail

The rain rates are high in the Tropics, so strong echoes are often returned from convective storms. However, during build-up and breaks, hail particles can be present in the convective storm clouds (May et al., 2000).

2.4.2 Error sources

Karlsson (1997) describes common error sources, which will be briefly described in the following. One error source arises from the curvature of Earth, which causes *radar beam overshooting*, as the pulse travels further away from the radar. The overshooting effectively sets a spatial limitation of the radar coverage area. Usually, distances larger than 250 km are not relevant. Another error source is related to conditions under a precipitating cloud, due to *low-level evaporation* of precipitation if the conditions are very dry below the cloud. The radar then overestimates the rainfall reaching surface. The effect of *bright band* has been mentioned earlier. This phenomenon is often distinct. An error, which should not be very common in the tropical region of northern Australia, is that of *absence of large droplets*, related to the 6-th power dependence of the diameter. Perhaps one of the most serious sources of error in the radar context is that of *anomalous beam propagation*. It is caused by anomalies in vertical profiles of atmospheric refractivity. Anomalous propagation (ducting) enables objects on the ground to return strong echoes, whereas sub- and super-refraction cause uncertainties in the vertical position of the radar beam. Another important error is that of radar beam *attenuation*. As long as the return signal is stronger than the noise signal always present, a radar signal can be detected. A minimum detectable signal (MDS) is the weakest echo that can be distinguished

from noise. Effectively, distance attenuation and attenuation by primarily hydrometeors (possibly severe in hail or heavy rain) will reduce the signal strength to below the MDS at large distances. Other sources of error to be aware of are radar echoes from *side lobes*, *screening by topography*, *flare echoes*, *multi-trip echoes*, *insects* and *propagating air mass boundaries* (such as sea breezes and cold pools sometimes associated with dusty gust fronts). It is anticipated that the error sources outlined will not affect the statistics for longer time scales, but might be important in individual radar scans during certain events.

2.4.3 Radars used in this study

The radars that have been used in this study are primarily the Gunn-Point located at the coast north of Darwin, and Berrimah (back-up) radar, located just southeast of Darwin. Figure 2-4 shows the locations of the radars. The Berrimah radar is a Doppler radar, whereas the Gunn Point radar is a polarimetric radar with a greater sensitivity, since it is also used for microphysical studies of clouds. In this study, the radar data used have been in the form of 3D volumes, which have been processed to create horizontal cross-sections at different altitudes, i.e., so-called CAPPIs (Constant Altitude Plan Position Indicator). These are composite radar displays constructed from radar data from many PPIs (Plan Position Indicators) at successive elevation angles, to obtain the pattern at a specified constant altitude. The C-pol radar runs a volume scan out to a radial range of 150 km every 10 minutes, through a series of plan position indicator (PPI) sweeps at a sequence of increasing elevations (May and Keenan, 2005). Since this report seeks to reveal features in the convective behaviour of the 2005/06 wet season, reflectivities less than 15 dBz have been discriminated. The CAPPIs were created based on 18 heights (2-19 km) and with a vertical and horizontal resolution of 1 km. A great simplification in organising the statistics from CAPPIs for the period of study has been provided by a technical system called TITAN.

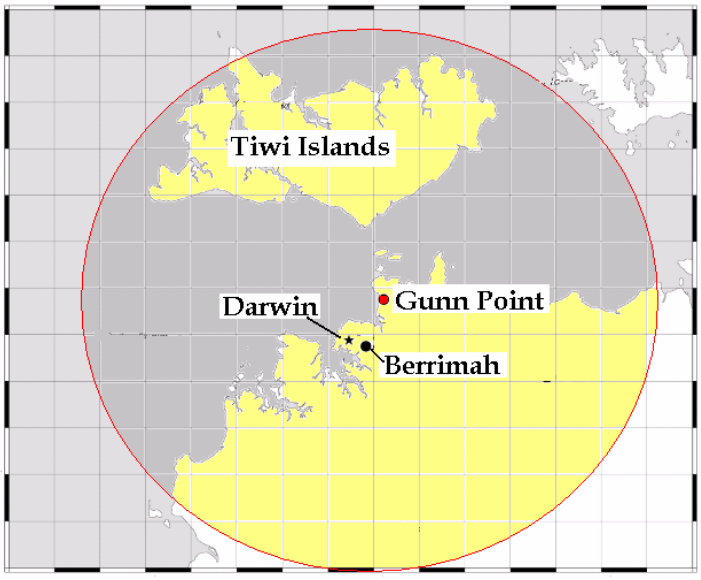

Figure 2-4. Gunn Point radar (centre) and its associated radar coverage zone.

2.4.4 TITAN

The TITAN (Thunderstorm Identification, Tracking, Analysis and Nowcasting) system started as a tool for the evaluation of cloud seeding programs, but has since grown to become a multidimensional tool for the analysis of convective storms making direct use of radar data (Dixon, 2005). It allows for the analysis of thousands of cells and months of data, which would be extremely tedious to analyse manually. It is used to track convective storms, which are defined as contiguous volumes of pixels that exceed a predefined reflectivity threshold (here 35, 40 and 45 dBz). To avoid noisy data, the cell volumes need to exceed a nominal limit of 30 km^3. Since the storms are identified at discrete times (every 10 minutes), an optimization procedure is employed to match the identified storms at a certain time with those at the next time step, as described by Dixon et al. (1993). Special functions handle mergers and splits. All cells are approximated with ellipses, which makes it possible to define orientations of the cells. The 35 dBz threshold covers most of the convective activity in the region, while the 45 dBz sorts out the most intense storms. The lower threshold is low enough to include areas of non-convective, i.e., stratiform precipitation. However, Ballinger and May (2005) showed that during the wet season in Darwin 2003/2004 only ~4% of the storm tracks showed at least one discrete time of stratiform classification. Therefore, this contribution to the total number of records will not be discriminated in the analysis.

The discrete tracking of the cells, with a time step of 10 minutes, makes it possible for cells to be erroneously tracked, especially during strong wind situations. Although the lifetimes of most convective clouds are longer than 10 minutes, many cells appear just once in the records as they only reach the cell detection threshold for a short time. Misidentifications are also possible. The fraction of storm records occurring only once was similar between the 35 and 45 dBz cases as observed by Ballinger and May (2006), who expects the cases of misidentifications to be relatively rare. Convective cells with intensities close to the set reflectivity thresholds might oscillate between the records, which can affect the analysis. Ballinger and May (2006) once again suspect these cases to be relatively few.

2.4.5 Data

In appendix B, the storm characteristics, as defined by a set of variables as collected by TITAN, are listed. The most important variables in this study are (except from the spatial and temporal properties of the storms) max reflectivity, speed and direction of propagation, orientation and echo top heights (as defined by the 35 and 45 dBz thresholds). A number of programmes have been developed to produce different types of statistics, in order to give a picture of the convective activity during the wet season 2005/06. Important assumptions and possible implications in the results will be explained when necessary.

Chapter 3

Analysis

The extensive dataset from the 2005/06 wet season will now be examined in further detail. First, an overview of the whole wet season convective characteristics will be presented. Differences between the 35 and 45 dBz cells under different regimes including the build-up, monsoon and break periods will be analysed. Then features of the regimes, such as convection under different shear regimes, mergers and splits versus isolated cells, squall-line versus non-squall-line cells and Hectors versus non-Hectors will be described and compared. The statistical significance of some of the observations will be tested in section 3.7.

3.1 Overview

3.1.1 Classification of Regimes

The wet season of 2005/06 has shown a typical high degree of variability, including periods of torrential rainfalls, dry spells, easterlies, westerlies, squall-line passages, stratiform rain events, MCSs and monsoonal depressions. These events are favoured by different atmospheric conditions, which can be classified as different regimes. The key parameter to analyse in this context is the wind. A commonly used method to distinguish between build-up/breaks and the monsoon, which will be applied here, is to simply use the zonal wind at a single (low) level (Drosdowsky, 1996). A westerly component in the wind corresponds to monsoon conditions, whereas an easterly component is associated with build-up/breaks. Figure 3-1 shows the wind conditions over Darwin at the 700 hPa level. This level has been chosen to show the low-level wind, but is high enough so that the influences of sea breezes and the heat-low are eliminated since these can be found at lower levels due to their shallow nature. It is evident that the period from November 17 to December 25, except from a few days in the very beginning, was characterised by easterly winds. The westerly burst in the beginning of the period will be excluded in the analysis, since this did not correspond to a real onset of the monsoon as there was no cross-equatorial flow. This feature has been observed many times, and is associated with synoptic scale disturbances (Drosdowsky, 1996). The figure suggests an onset date to be on December 26 although a strong westerly regime is not obvious until January 12. However, the weather that coincided with the period following December 26 was consistent with that of a typical monsoon (abundant convection, large areas of precipitation, little lightning, overcast). The streamline analysis showed that the flow originated in the northern hemisphere, typical of the monsoon. Since the wind speed was low, it is likely that the monsoon trough was positioned over the northern Top End, also explaining the abundant convective activity at this time. A surface trough implies rising motion at low levels, acting to minimise CIN.

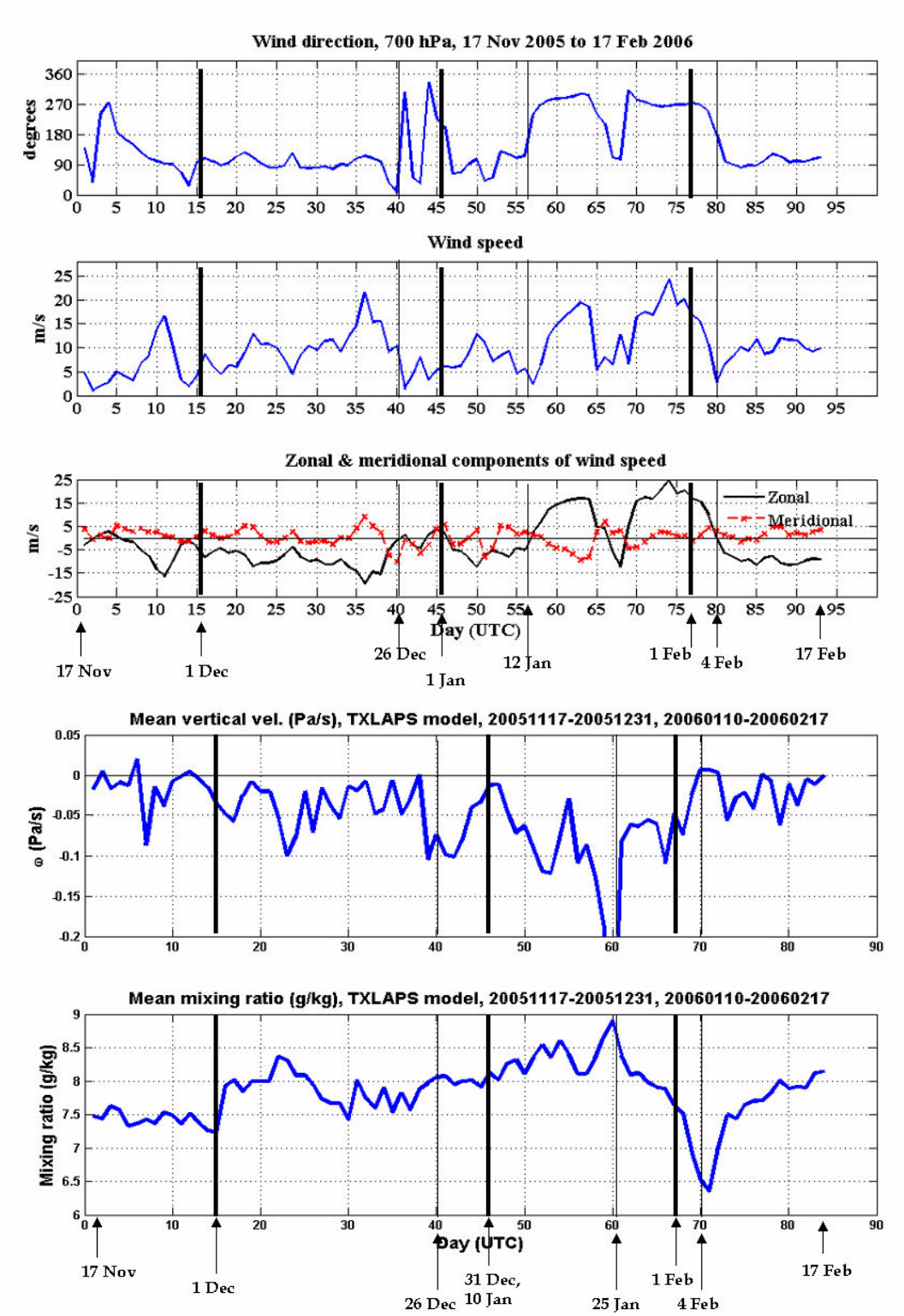

Figure 3-1. The three top graphs show the wind direction (counted clockwise from north) and speed at 700 hPa, 17 Nov. 2005 to 17 Feb. 2006, and the associated zonal and meridional components. The x-axis represents the day number with day 1 = 17 Nov 2005. Thick lines represent the first day in each month (Dec., Jan. and Feb.). Thin lines represent days that are mentioned in the analysis. The two bottom graphs show spatially and temporally averaged vertical velocity (Pa s^{-1}) and mixing ratio (g water per kg air) respectively, with a data gap between Jan 1 and Jan 9, 2006. All data are based on soundings and TXLAPS diagnosis.

The vertical wind has been diagnosed and the mixing ratio (mass of water per kg air) analysed through the troposphere by the TXLAPS model. TXLAPS is an extended version of the operational numerical weather prediction LAPS model developed at the BMRC, customised to cover the tropical atmosphere. The output for this specific case is based on five grid points in the vicinity of Darwin and has been averaged in space and time on a daily basis, and can be seen in figure 3-1. Data are missing for the first ten days of 2006, but cover the period of November 17 2005 to February 17 2006. The vertical velocity is in pressure coordinates ($Pa \cdot s^{-1}$), which accordingly implies rising motion when the values are negative (pressure decreasing with time) and subsidence when positive. It is clear that the vertical velocity increased at day 39, i.e., the 25th of December, which supports the suggested position of the monsoon trough and associated increase in convective activity. However, there is no distinct signal in the mixing ratio, which only shows a weak increase in water content (~0.5 g water/kg air) through the depth of the troposphere.

The increase in upward motion seen around January 25 was caused by a mesoscale convective system with an associated vortex that moved westwards over the Top End. Another observation is the extensive drying and mean subsidence through the depth of the troposphere around February 4. Convection was almost absent during these suppressed conditions before the easterlies strengthened and the continental convection was activated. With an onset date of the monsoon set to the 26th of December, the preceding period can be characterised as a build-up period. However, the monsoonal burst was short, and break conditions can be identified in the wind direction between January 2 and January 11, followed by a classic monsoon between January 12 and January 24. The subsequent drier period with very strong winds of gale force strength is characterised as a "dry monsoon" for reasons that will be clear in the following analysis. The suppressed period around February 4 marks the beginning of the break period lasting until the end of the period of study. Table 3-1 summarises the discussion.

Table 3-1. Characterisation of the wet season 2005/06.

Period	Regime	Day of study
20051117-20051225	Build-up	1 -39
20051226-20060101	Monsoon	40-46
20060102-20060111	Break	47-56
20060112-20060124	Monsoon	57-68
20060125-20060204	Dry Monsoon	69-78
20060205-20060217	Break	79-93

Figure 3-2 shows the mean vertical velocities ($Pa\ s^{-1}$) separated into the different regimes. It is evident that the monsoon shows a mean ascent of air through the depth of the atmosphere peaking in the mid-troposphere. The break periods show slightly more suppressed conditions than the build-up and dry monsoon, although it should be kept in mind that the differences are small and based on model diagnosis. There is a general tendency toward rising motions through the troposphere throughout the wet season, which can be explained in terms of low-level convergence and upper

level divergence. Another important observation is that the monsoon shows generally moister conditions than any other regime, with mixing ratios 1-2 g·kg^{-1} higher in the mid-troposphere, which is consistent with the study by McBride and Frank (1999). This reflects the upward motion of air with oceanic origins and the abundant convection.

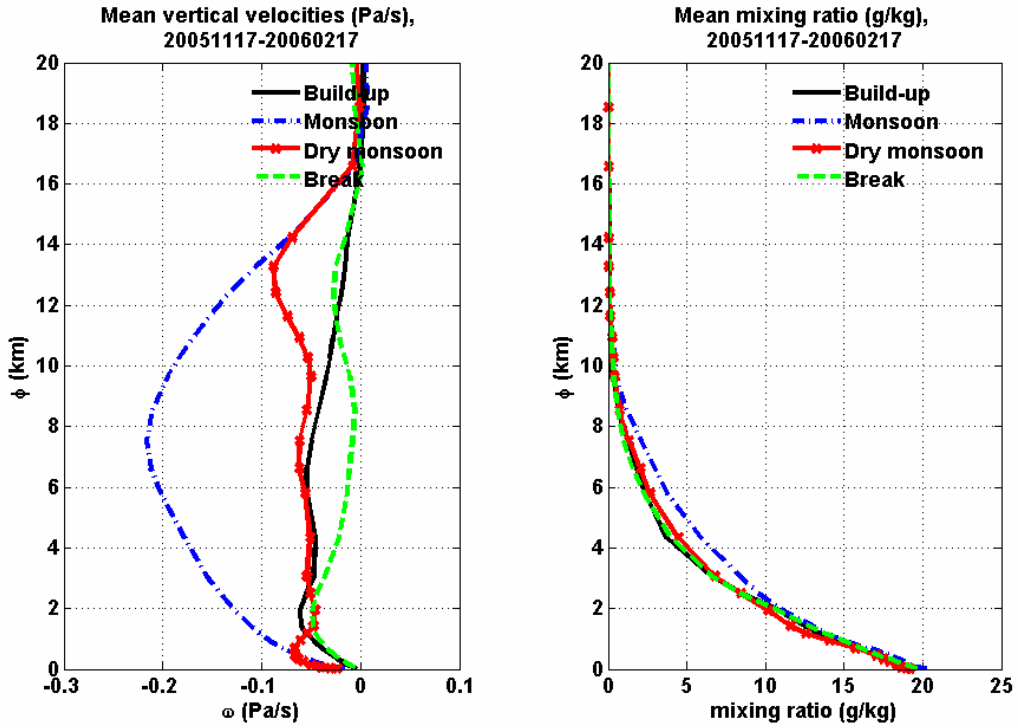

Figure 3-2. Mean vertical velocities (Pa s^{-1}) and mixing ratio (g kg^{-1}) for the different regimes averaged in space and time for five geographical locations (= grid points) close to Darwin based on analysis from the TXLAPS model November 17, 2005, to February 17, 2006. The y-axis represents the geopotential height (denoted Φ) in km (≈ altitude). The vertical velocity in pressure coordinates is denoted ω.

3.1.2 Occurrence of convection

Figure 3-3 shows the number of 35 and 45 dBz cells, and the number ratio of 45 to 35 dBz cells per day, as well as the average area fraction covered by these cells per hour during the day. A quick look at the number of cells exceeding 35 dBz reveals that the first 40 days, i.e., the build-up period, shows approximately 150 cells/day, followed by 35 days with numbers in the vicinity of, or exceeding 200, cells/day. These numbers are based on single tracks, i.e., not taking into account merges or splits. Except from a few days with intense activity (Dec. 24 and Jan. 12-15), the 45 dBz threshold does not show the same pattern as the 35 dBz threshold during this period. This is indicative of the more general upward motion through the troposphere during the monsoon, favouring widespread, but less intense, convection than during build-up and breaks. Consequently, the ratio of number of 45 to 35 dBz cells drops during the 35-day monsoon period (including a short break) as compared to the preceding and subsequent periods. Simultaneously, the average area coverage

of pixels exceeding a reflectivity of 35 dBz to the radar coverage area shows *an increase* during this period.

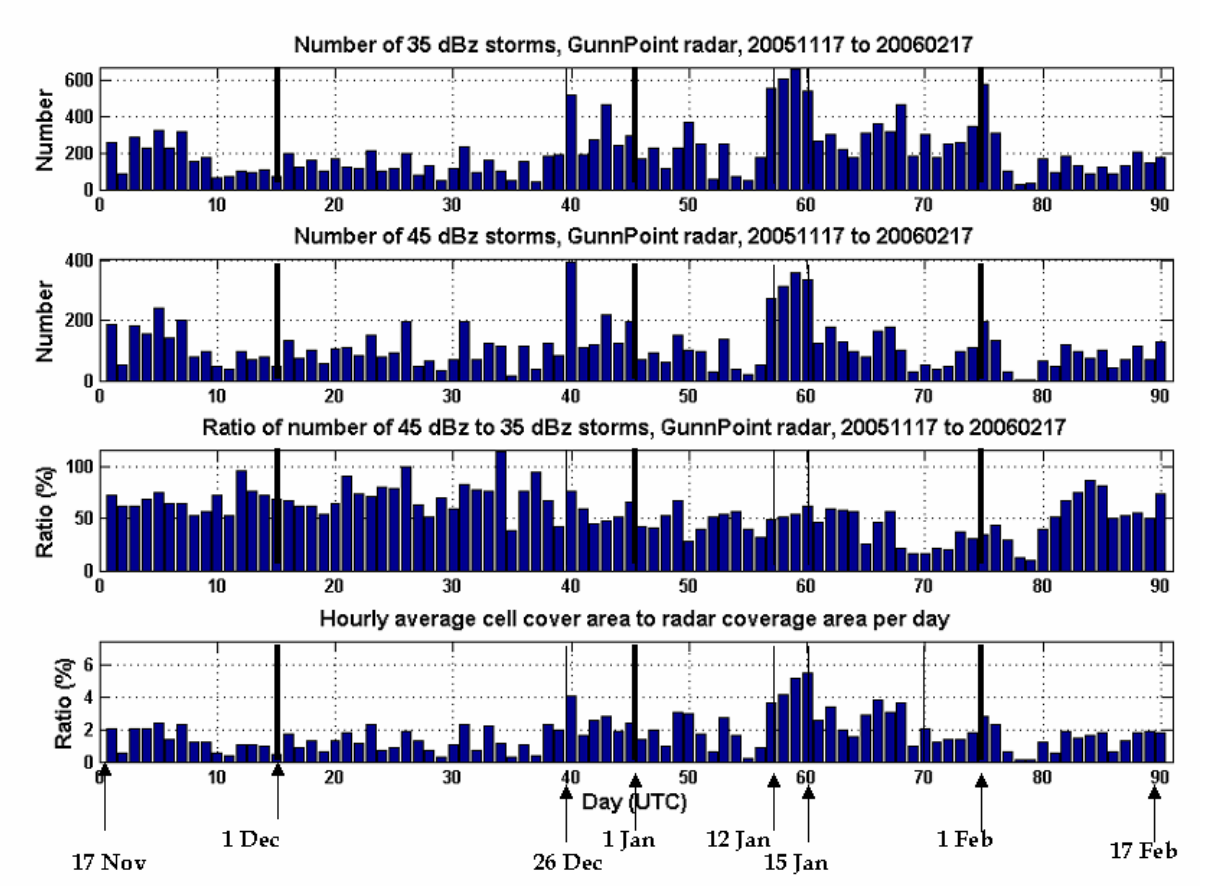

Figure 3-3. The topmost graph shows number of 35 dBz followed by number of 45 dBz cells as identified by TITAN and their number ratio (3rd graph), on a daily basis. Average area fraction covered per hour each day is shown in the bottom barplot.

This demonstrates the requirement during break conditions for stronger forcing, but when the potential instability has been locally released, deep and intense convection can develop. This explains the observed higher ratio of number of 45 to 35 dBz storms during the build-up and break periods.

The horizontal and vertical distributions of different reflectivities with time are indicative of the convective activity in the region and can be deduced from figure 3-4. It shows the maximum area covered by specified thresholds as a function of time (starting on December 8, 2005) and height. It is based on CAPPIs and shows the maximum coverage at a given height per day. Two reflectivity thresholds have been used; 15 and 35 dBz (refer to table 2-1). The 35 dBz threshold shows generally low values which is expected due to its general dependence on convective updrafts. December 17 shows an areal coverage exceeding 30% of the radar zone for the 35 dBz threshold at low levels, making it one of the largest event of the summer. The 15 dBz threshold shows values in excess of 90% at low levels. This is an example of a mesoscale convective system and the associated stratiform precipitation. A similar scenario developed during December 24, two days before the onset of the monsoon.

An example of deep convection is that of January 10, which shows top heights of the 35 dBz threshold in excess of 14 km. A closer look at the CAPPIs for this specific day reveals areas with 45 dBz echoes at this height. This is an indication of deep convective cores embedded in the larger area of convection of different phases. The Darwin sounding from 00UTC (LT= UTC + 9½ hours) on January 10 showed a deep moist layer, especially at levels above 700 hPa, and CAPE values close to 1500 Jkg^{-1}. McBride and Frank (1999) found that the average CAPE values for the active periods were in the order of 1700 Jkg^{-1}, whereas breaks showed values in excess of 2000 Jkg^{-1}. The system of January 10 preceded the second monsoonal burst. A typical CAPPI from the monsoon period following January 10 is seen in figure 3-5. It shows the areal distribution of radar echoes at 2 km height. This figure will be referred to in the discussion of the monsoon. Another feature of figure 3-4 is the great coverage for all reflectivity thresholds on January 24, a day which was characterised by the passage of a monsoon MCS with developing tropical storm characteristics. This marked the onset of the dry monsoon that lasted for more than a week with an associated strong westerly wind at low levels. The following ten days were characterised by shallow and small-scale but frequent convection. A couple of convectively inactive days were then followed by a classic break period, once again showing high echo tops for all the reflectivity thresholds.

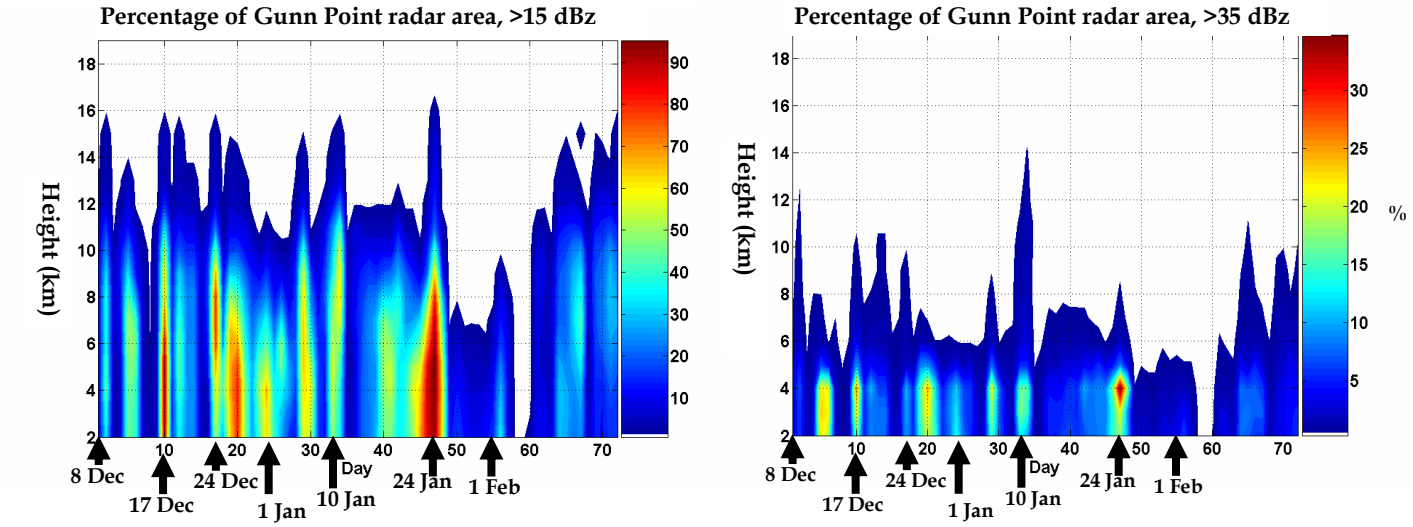

Figure 3-4. Percentage of radar coverage area taken up by reflectivities exceeding 15 and 35 dBz as a function of time and height, based on CAPPIs from Gunn Point radar. The x-axis gives the day number, starting on December 8. The y-axis shows the height in km.

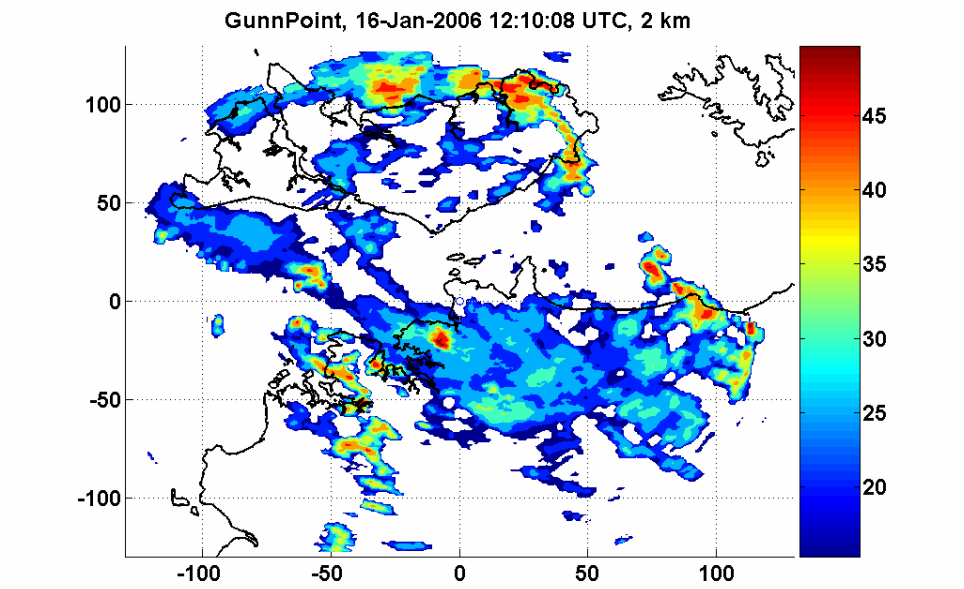

Figure 3-5. Gunn Point CAPPI at 2 km height from 12 UTC January 16, 2006. The scale shows the reflectivities in dBz and it is clear that convective cores are embedded in larger areas of stratiform precipitation, which is typical for monsoonal conditions.

3.1.3 Height distribution

The height distribution of cells as defined by 35 dBz echoes, i.e., the distribution of precipitating hydrometeors and not cloud top heights, will now be examined using TITAN data. Figure 3-6 shows the distribution of storm top heights as defined by the maximum height of the 35 dBz echoes for individual records. It shows the frequency of occurrence based on daily observations. One distinct feature of the figure is the preferred 35 (and 45) dBz echo top heights at around 7 km. The results point towards a rather continuous single-peaked distribution of 35 dBz echoes. An exception from the 7 km peak in frequency of occurrence is found in the dry monsoon, which shows generally lower 35 dBz echo top heights.

Another feature that can be seen in figure 3-6 is the presence of near-tropopause 35 dBz echo top heights during the build-up and break periods, which is almost absent during the monsoon periods. Once again, this might reflect the stronger forcing mechanisms required to initiate convection and the high-CAPE environment during the potentially unstable conditions that prevail during build-up and break periods. The discussion so far has indicated the differences in height distribution of cells between different regimes. In order to fully explain these differences, the temporal and spatial distributions of these cells need to be examined. This will be done for each of the regimes separately, since these will be seen to differ in terms of many observed properties.

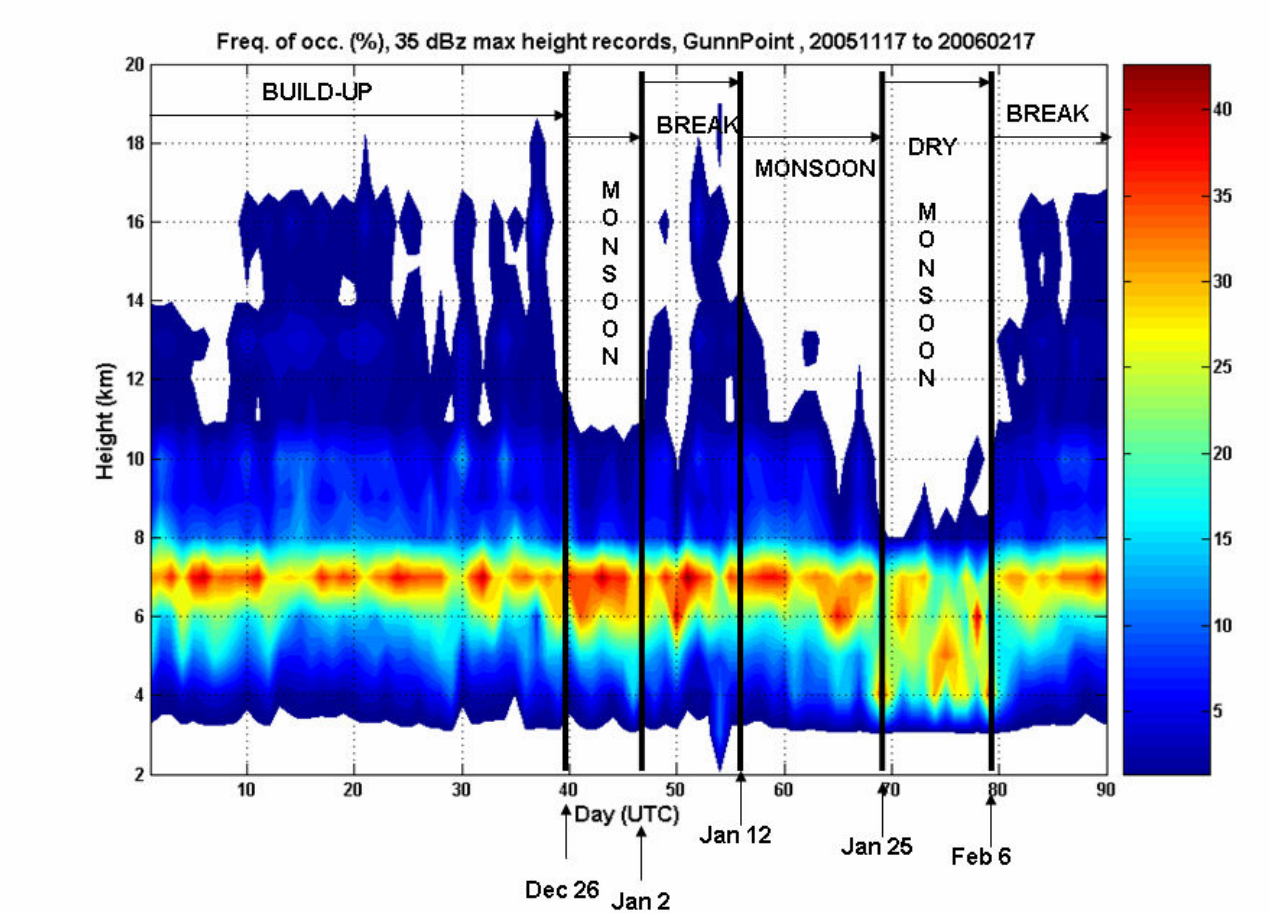

Figure 3-6. Frequency of occurrence of 35 dBz maximum echo top heights during the wet season 2005/06. The x-axis shows the day number with day 1 corresponding to November 17, 2005. The thick lines separate the different regimes identified earlier. The graph is based on daily records, i.e., the percentage of cells reaching a certain level for each day. Based on data from TITAN.

3.2 Build-up and breaks

Convection is a response to imbalances in the atmospheric environment. These follow diurnal cycles and depend largely on low level characteristics as outlined in chapter 2. Figure 3-7 shows the distribution of number of cells as a function of hour of day. It shows one distinct peak and one less obvious secondary peak in the distribution of cells during the course of the day. The primary peak is found during the midafternoon, at about 5 UTC, i.e., 14.30 LT, and the smaller peak at around 20 UTC (05.30 LT). The build-up and break regime showed about 4 times as many cells at the day peak as at the night minimum, confirming the strong diurnal modulation of convection. These peaks are evident also for the 45 dBz threshold. To explain the presence of two peaks, we need to recall the location of Gunn Point radar, which covers both oceanic and continental regions. These show different temporal distributions of cells, as is evident in figure 3-8, showing the spatial distribution of cells at different times of the day. The numbers on the scales represent the number of cells with a storm centre located within a grid square of 10x10 km^2 for the radar coverage zone.

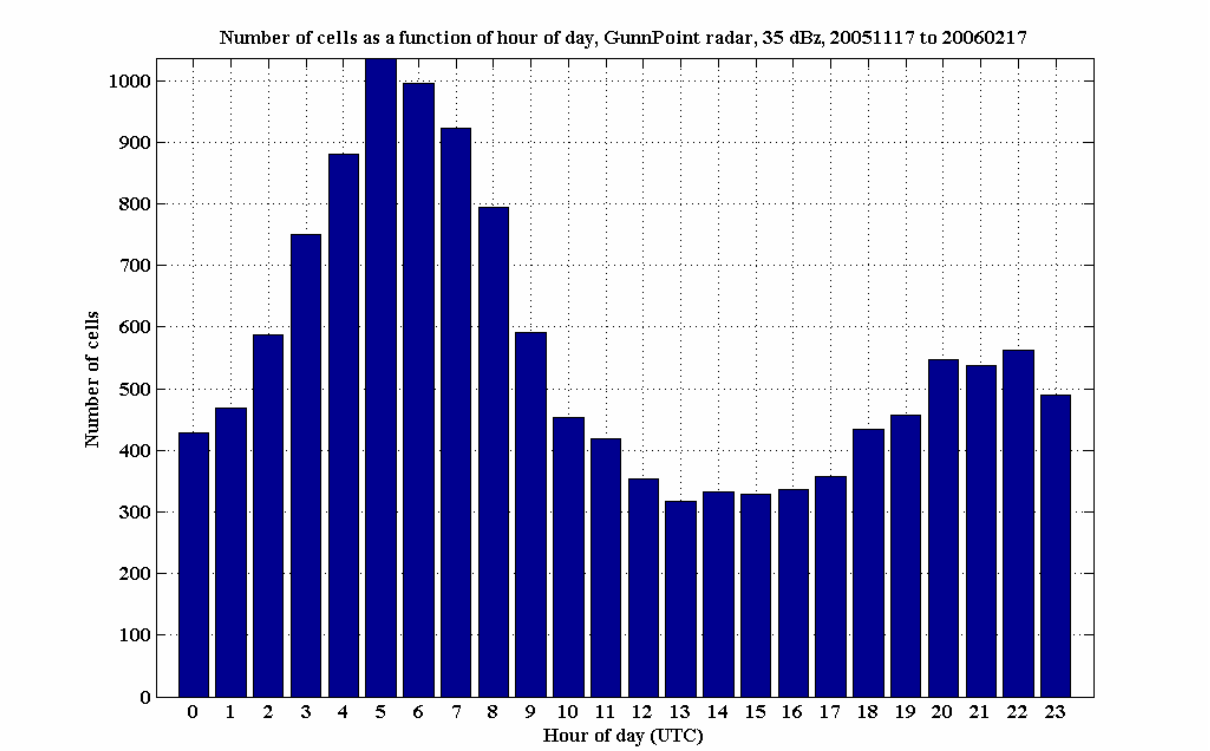

Figure 3-7. Total number of cells during the build-up and break periods as a function of hour of day as observed by Gunn Point radar and tracked by TITAN, 35 dBz threshold.

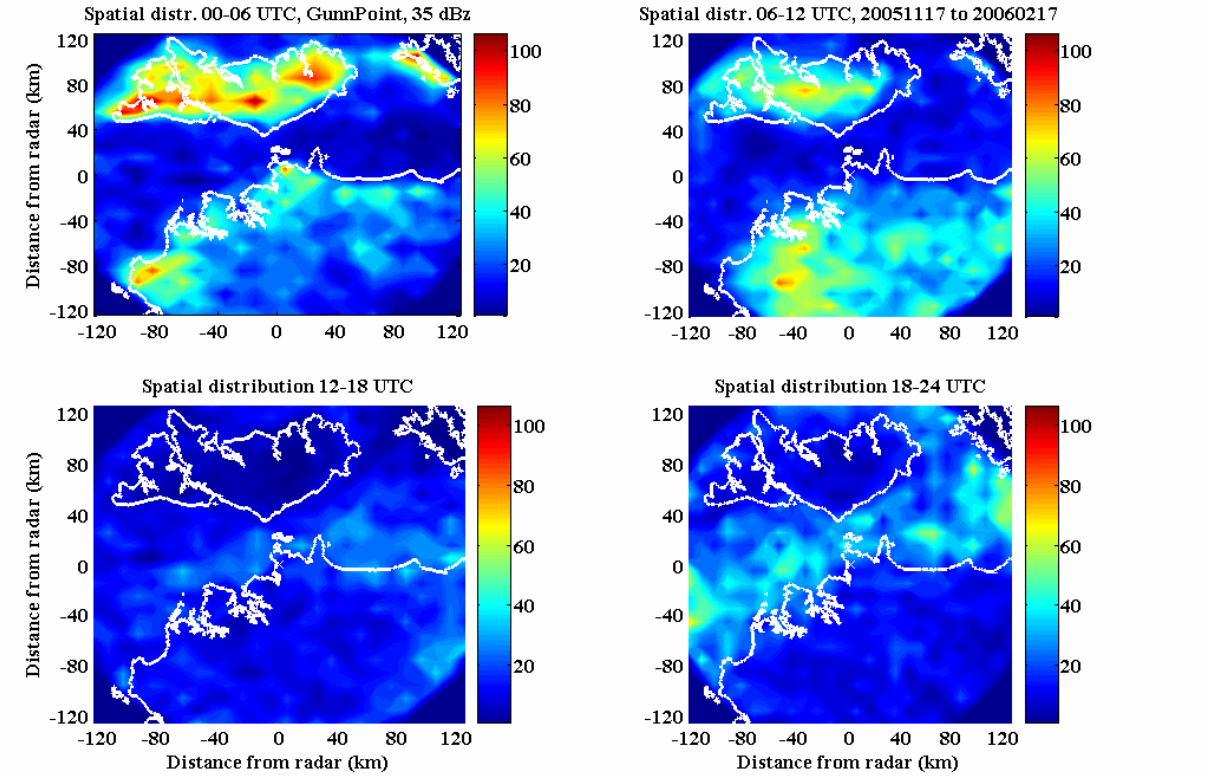

Figure 3-8. Spatial distribution of 35 dBz cells subdivided into four 6-hour blocks of the day for Gunn Point radar during build-up and breaks. The scale bars to the right of the graphs show the total number of cells that have been centred within a 10x10 km² grid square. Based on TITAN data.

The midday plot (00-06 UTC) shows a strong peak over the Tiwi islands, reflecting the climatological signal in the presence of Hectors as well as a pronounced coast-aligned line of more frequent convective activity. These peaks indicate the importance of sea breezes (Wilson et al., 2000), especially since convection is quite sparse further inland over the continent. The subset of intense cells (45 dBz) shows an even more distinct peak at the Cox peninsula to the southwest of the radar, not as evident for the 35 dBz threshold.

At 06-12 UTC, i.e., late afternoon and early evening, a distinct north-south oriented line of enhanced convection can be seen at around x = -40 km, i.e., 30-60 km from the coast. Isolated cells have formed inland at this time and show a rather uniform distribution. Simultaneously, the intense convection over the Tiwi islands has eased and moved towards the northwest in the mainly east-southeasterly flow prevailing during this regime. This observation might be an indication of the observed evolution of sea breezes and Hectors.

At night (12-18 UTC) the picture has changed dramatically, with the Tiwi islands showing the least convective activity in the region. This is not surprising, since the island has been cooled by late afternoon storms and cold pool production. A developing land breeze circulation with a descent of air and decaying convective cloud remnants clears the skies. On the other hand, this phenomenon might activate some convective activity around the island, seen in a gradient in occurrence of records close to the islands. The same pattern is not as clearly seen in the 45 dBz cell distribution, reflecting the possible observation that convection with oceanic origins is weaker lacking the strong forcing and deep boundary layer seen over land at daytime. Despite this observation, the cells occurring over the water closer to the mainland show a more distinct peak in distribution. These cells might be the result of land breezes and squall-lines moving offshore, as has been seen in some radar loops. Squall-lines are evident in the southeastern corner. The formation of convective lines is such a characteristic feature of the build-up and break that it deserves some further examination, which will be outlined in section 3.2.2.

The morning is characterised by decaying convection offshore and is perhaps the least interesting feature of the diurnal convective cycle, although some of these showers occasionally move in over coastal locations such as Darwin.

3.2.1 Hectors

The ideal environment for convection and strong forcing over the Tiwi islands, as outlined in section 2.3.3, might support different convective characteristics to that found over the continent. However, the height distribution of 35 dBz cells does not show any strong difference between the subset of storms occurring over the Tiwi islands to those occurring over the continent. There might be a slight tendency towards higher storm tops over the continent, but this will be statistically analysed in section 3.7 along with other observed characteristics. The observed orientation with

respect to low-level shear is nearly uniformly distributed, with a slight tendency towards a 45° angle, possibly reflecting the transition from a zonal to a meridional orientation of the convective cells with time, as found by Keenan and Carbone (1992). This type of transition in orientation can be seen in figure 3-9, showing three CAPPIs at 05, 06 and 07 UTC, during a typical break day. The orientation with respect to shear found over the Tiwi Islands is not seen for records outside the Tiwi islands for the same time period (03 to 09 UTC, i.e., 12.30 to 18.30 LT), which has a strong bias towards shear-parallel orientations. However, if all cells occurring over the continent at all times are included, there is a bias towards orientations that are perpendicular to low-level shear. It can therefore be suspected that a transition from shear-parallel to shear-perpendicular cells occurs on a diurnal basis. The effects of shear will be further examined in section 3.5.

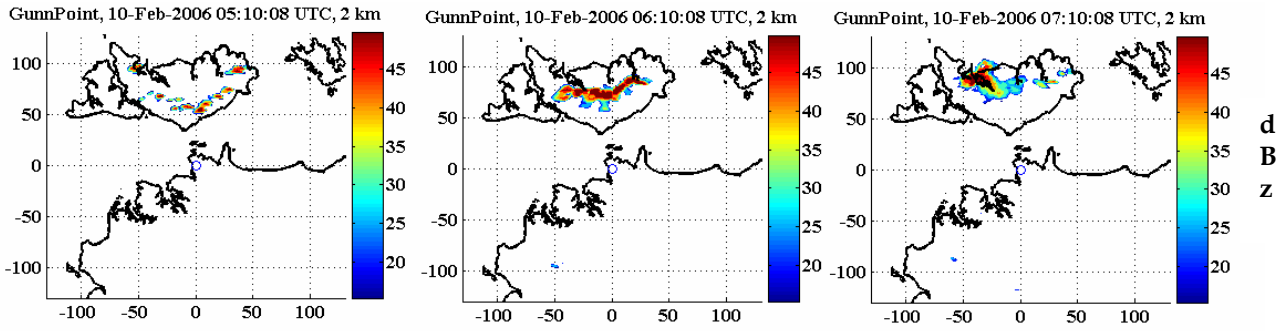

Figure 3-9. Gunn Point CAPPIs from 05.10, 06.10 and 07.10 UTC, February 10, 2006. The x- and y-axis indicate the distance from the radar. The scale to the right of the graphs represent the reflectivity values (dBz). Note the transition from a zonally oriented line of convection towards an arc-shaped more meridional complex.

To summarise the observations, it can be concluded that the initial storms seem to favour sea-breeze front alignment (as seen in figures 3-8 and 3-9), then being dictated by interactions of cold pools and with the shear such that the system tends to become more shear-perpendicular with time. This is in line with the theory outlined in chapter 2.

3.2.2 Squall-lines

Figure 3-10 shows a classic squall-line at 12 UTC with a westward propagation on December 24, 2005. The reduction in reflectivities and spatial distribution of echoes at 13 UTC might be explained by a wet radar radome or attenuation. A trailing stratiform region developed several hours later (15-18 UTC). The CAPPIs suggest a speed of the squall-line on the order of 40-50 kmh^{-1} (11-14 ms^{-1}). This is just below the speed of the ambient flow at 700 hPa (~15 ms^{-1}, see figure 3-1) and the squall-line is nearly orthogonal to the flow. The last two subplots show the area coverage of pixels exceeding 15 and 35 dBz. By about 17 UTC, more than 70% of the radar coverage zone was covered by reflectivities exceeding 15 dBz at 6-8 km height, which is possibly indicative of a thick and extensive cloud anvil.

The initiation mechanisms for convection are fundamental to configure convective lines, but they do not explain why and how convective lines are sustained. The conceptual model of Houze (1993) seems to work well for this squall-line. The wind shear vector pointed westward and was rather strong, around 10 ms^{-1} as evident in figure 3-13, along with the presence of rather dry mid-level air. This was indicated by a Darwin sounding from 12 UTC on December 24, and effectively supports the formation of cold pools through evaporative cooling that acts to enhance the convection on the front side of the propagating squall-line. The slightly slower translation speed than the ambient flow at 700 hPa is probably caused by the high shear at this time, as discussed by Keenan and Carbone (1992). The rather similar reflectivities over ocean and continent despite of the nocturnal conditions, clearly indicate the presence of non-diurnal forcing mechanisms maintaining the system. The accumulation of old cells forming a region of stratiform appearance is clearly seen after a few hours, as opposed to the original intensifying stage, which lacks the stratiform region.

The formation of an arc-shaped bulge at 15 UTC is in line with observations of convective lines under strong low-level shear and relatively weak mid-level shear, as found by LeMone et al. (1998). It might also be indicative of bursts of the easterly momentum at 700 hPa down to the boundary layer in a rapidly forward-spreading dense cold pool. The presence of dry midlevel air favours the development of intense downdrafts, as has been discussed earlier.

There are several other types of squall-lines than the classical one described. Often, the conditions are such that discontinuous propagation is favoured (Keenan and Carbone, 1992). An example of this type is when forward spreading cold pools move faster than the environmental flow. This type of convective line could be expected to be more common during situations with dry mid-levels (Keenan and Carbone, 1992). Similar systems were observed also during the dry monsoon, although these lines at times tended to be rather two-dimensional. A third type of squall-line is that which forms on a pre-existing cold pool and was observed in some radar loops. A total of 38 squall-line cases were chosen to explore any differences in cell characteristics as compared to cells that were not part of the squall-lines. The differences between subset of cells will be discussed in section 3.7.

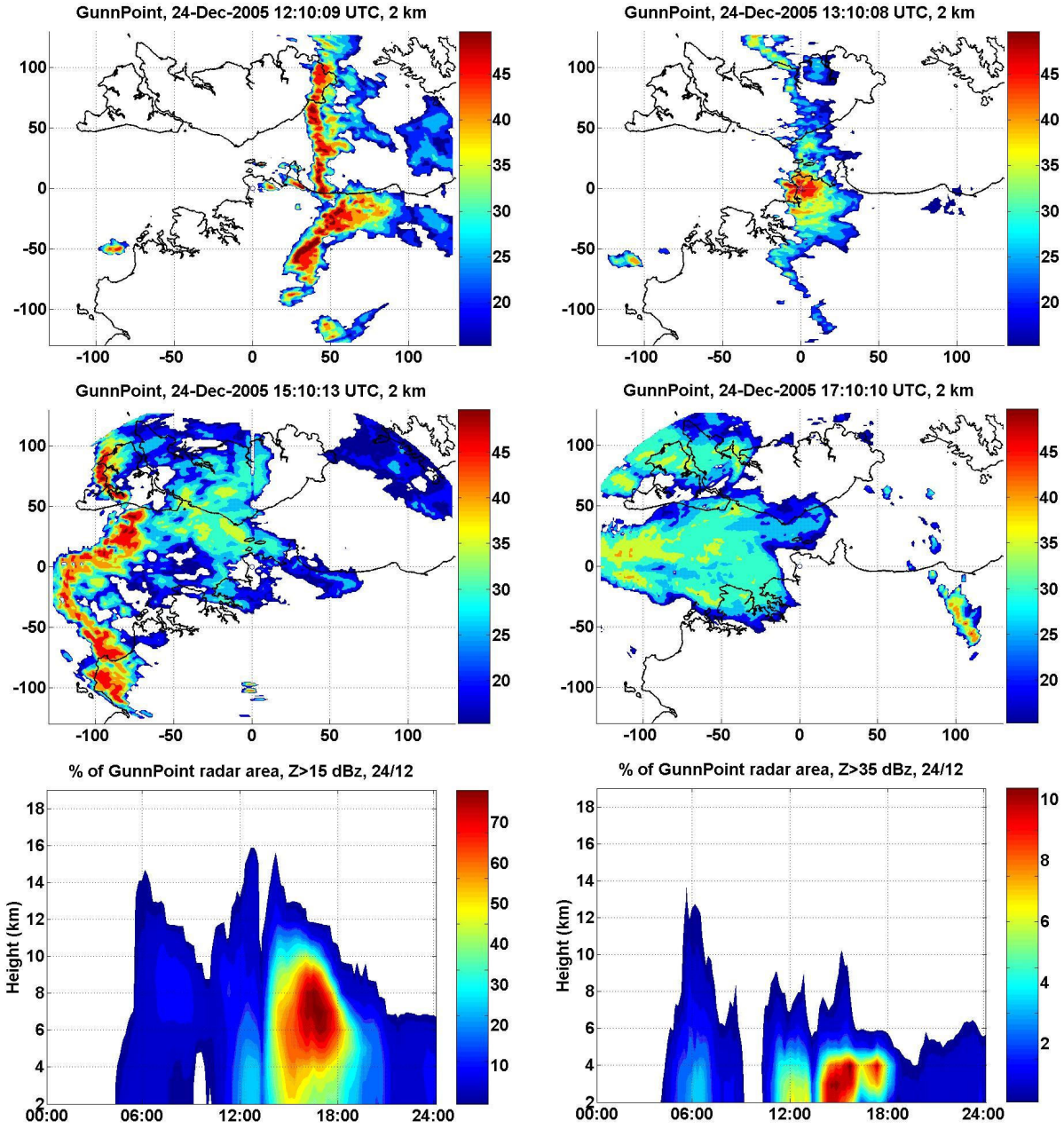

Figure 3-10. A squall-line passed through the Top End including the Tiwi Islands on December 24, followed by stratiform rain. At 13 UTC, the squall-line was nadir to the radar and the radardome was wet. An arc-shaped formation developed after passing Darwin and is evident in the middle left figure. The topmost four graphs are CAPPIs with the x- and y-axes showing the distance from the radar. The scale to the right shows the reflectivities (dBz). The two bottom figures show the area percentage of the radar zone that was covered by reflectivities exceeding 15 and 35 dBz respectively. The scales show the percentage.

3.3 The monsoon

The monsoon was characterised by widespread convective activity in space and time, with more rainfall in the western sector, i.e., over the ocean and along the coast, as seen in the spatial distribution in figure 3-11. There was also a slightly enhanced

activity over land at daytime. However, compared to the strong diurnal modulation of the build-up and break convection (see figure 3-7), this signal is much weaker. The 45 dBz cells are seen to be more diurnal in their character with a peak in the midafternoon. The dominance of frequent relatively weak convection was reflected in the ratio of number of 45 to 35 dBz storms and in the lack of 35 dBz cells reaching the upper troposphere (figures 3-4 and 3-6). It was seen also in figure 3-2 that the mean vertical motion during the monsoon was enhanced through the depth of the troposphere, giving rise to less convective inhibition so that less forcing was required. The positive feedback mechanisms of convection, described by Houze and Mapes (1992, see section 2.3.2), precondition the atmosphere so that new convection occurs more easily. The convection originating over ocean differs from that over land, as can be seen, for example, in the average area that the 35 dBz cells cover (figures 3-4 and 3-6) and the height distribution. This confirms the observation by Keenan and Rutledge (1993) that oceanic convection tends to be weaker. An example of a typical monsoon day was seen in figure 3-5 (16 January 2006). Regions of intense rainfall were seen at some locations, but mostly the area was covered by widespread and quite moderate rainfall. It is evident that the echoes were confined to the lower part of the troposphere, since echoes were almost absent at 10 km and above. Small squall-lines can be found over the Melville Island, the north coast and to the southwest of Darwin, indicating their presence also in a monsoonal regime, showing more complex characteristics.

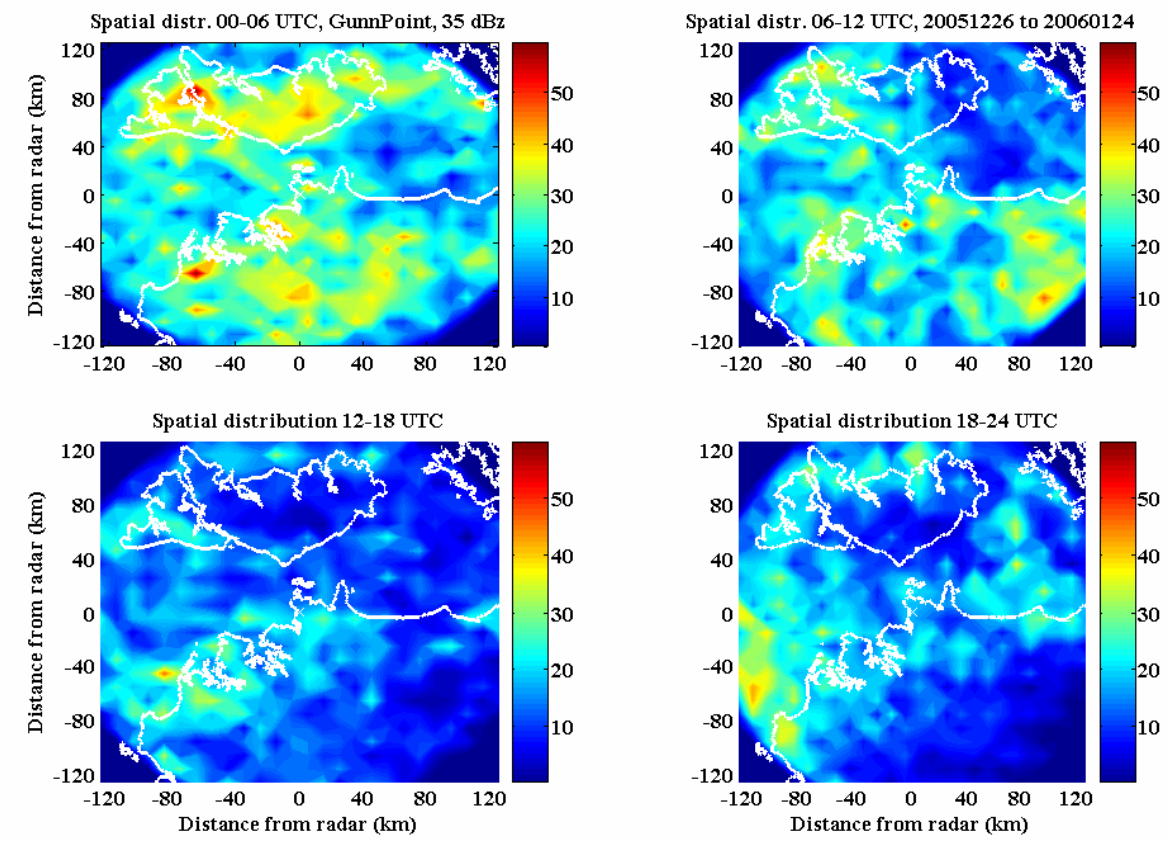

Figure 3-11. Spatial distribution of 35 dBz cells subdivided into four 6-hour blocks of the day for Gunn Point radar during the monsoon. The scale bars to the right of the graphs show the total number of cells that have been centred within a 10x10 km² grid square. Based on TITAN data.

3.4 The dry monsoon

The lower peak in the distribution of max heights between 4 and 7 km, as seen in figure 3-6, might be explained by the prevalence of dry air at relatively low levels, mostly confined to the region between 700 and 500 hPa (i.e., 3–6 km), as indicated by soundings from Darwin airport. The steady decrease in the mixing ratio during the dry monsoon is also seen in figure 3-1. Occasionally, dew points below -30 ^{o}C were observed at these levels. The reason for this was that dry continental air was wrapped around a low to the south. Entrainment and detrainment would in this case act to inhibit further growth through evaporation and associated cooling reducing the buoyancy. The existence of relatively strong wind shear through the dry mid levels (700-500 hPa) at this time during the dry monsoon would possibly favour the suggested influence of entrainment on cell heights.

Figure 3-12 shows the spatial distribution of cells. It is evident that an enhanced convective activity was found at daytime over the southern parts of the radar zone and the Tiwi Islands. This despite the short residence time of boundary layer air over the islands under the strong westerly winds that occasionally reached gale force along the coast. The oceanic character of convection can be seen in a double-peaked temporal distribution of cells for the ten days. The number of 45 dBz storms was low during this regime, but was enhanced during the period between January 30 and February 2, with a peak in occurrence on February 1. Although generally not reaching the tropopause, the convection was strong enough to produce reflectivities up to 60 dBz indicating the presence of large droplets.

The lack of sea breezes, the presence of dry air at midlevels and the only weak mean ascent compared to that seen during the monsoon (see figure 3-2) require other forcing mechanisms. The sounding from Darwin airport at 00 UTC on February 1 indicated moist boundary layer conditions with near surface dewpoints of 25 ^{o}C and CAPE-values of approximately 600 J kg^{-1} for an air-parcel raised from low levels, i.e., supporting rather modest cloud development, but a low cloud base, since the moisture content of the low level air was high. The lack of CAPE and moisture at mid-levels might explain the relatively low 35 dBz echo tops. The low-level moisture is possibly due to the intense surface fluxes of moisture from the ocean surface during the strong-wind regime (Houze and Mapes, 1992).

The existence of persistent lines of enhanced convection seen over the Tiwi Islands and to the south at 00-06 UTC, as well as along the north coast of the Top End at 12-24 UTC, cannot be explained on the basis of TITAN data. However, the dynamic forcing due to friction over the islands, and a slight orographic forcing together with a slightly warmer land surface, might possibly explain the enhancement seen over the Tiwi islands. Nevertheless, formations of convective lines generally depend on other mechanisms, such as wind shear interaction with convective cells. During the dry monsoon, there was a strong mid-level shear pointing westward and a weaker shear pointing eastward. LeMone et al. (1998) expect convective line formations that

are mid-level shear parallel in this kind of environment. This can be seen in the patterns in figure 3-12.

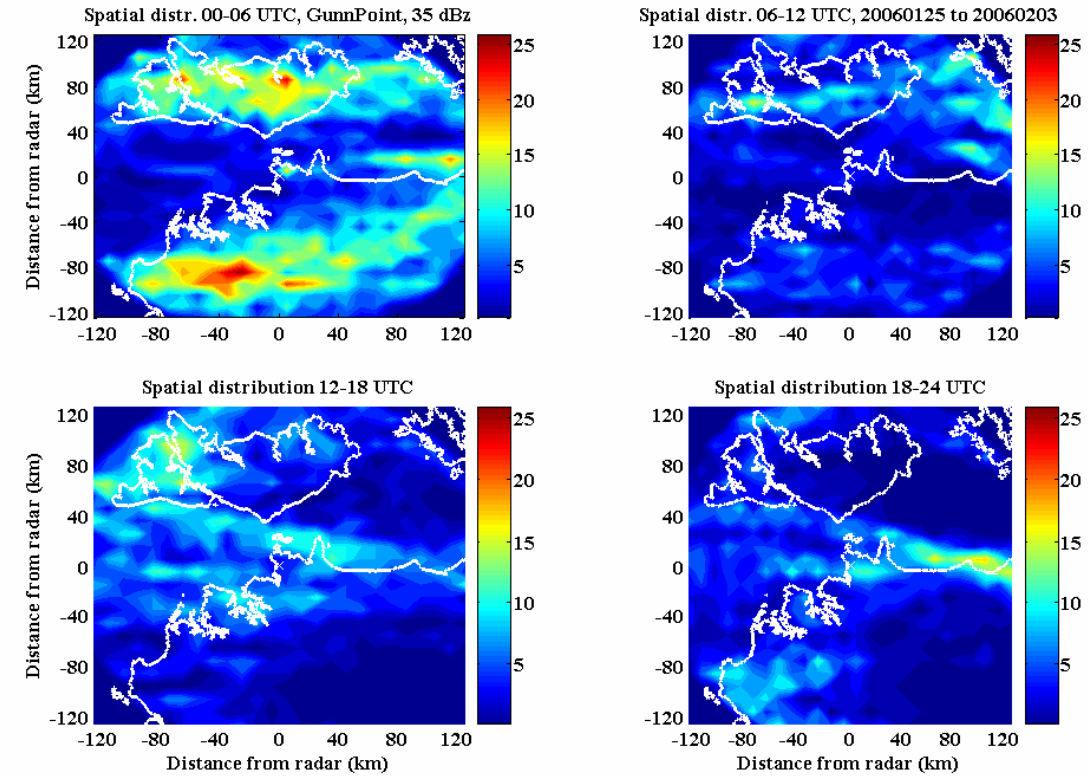

Figure 3-12. Spatial distribution of 35 dBz cells subdivided into four 6-hour blocks of the day for Gunn Point radar during the dry monsoon. The scale bars to the right of the graphs show the total number of cells that have been centred within a 10x10 km² grid square. Based on TITAN data.

3.5 Influence of vertical wind shear on cell orientations

In chapter 2, it was hypothesized that convective organisation is controlled largely by the vertical wind shear conditions at both low- and mid-levels. Therefore, we will examine the shear conditions in at least two layers, in order to test if the observed cell orientations are consistent with the hypothesis. Figure 3-13 shows the magnitude of the wind vector differences at the 850 - 700 hPa and the 700 - 500 hPa levels. Shear is defined as these vector differences divided by the depth of the layer. According to the regimes identified by LeMone et al. (1998) we could expect the following biases in the cell orientations with respect to shear (table 3-2). Note the overlap in some cases due to the compliance with more than one requirement.

The following discussion is based on orientation data from TITAN, i.e., individual cell orientations. However, in order to filter out line-like structures from essentially isotropic simple cells, a minimum ratio of 3 to 1 of the cell major axis to the minor axis has been implemented. It is reasonable to suspect that a cell that is elongated is so because atmospheric conditions are favourable for such a formation, and that wind shear might play an important role in this process. In addition to the TITAN

statistics, loops of the CAPPIs have been studied. Note that the 35 dBz threshold has been used, but that this threshold also includes embedded stronger convective cores.

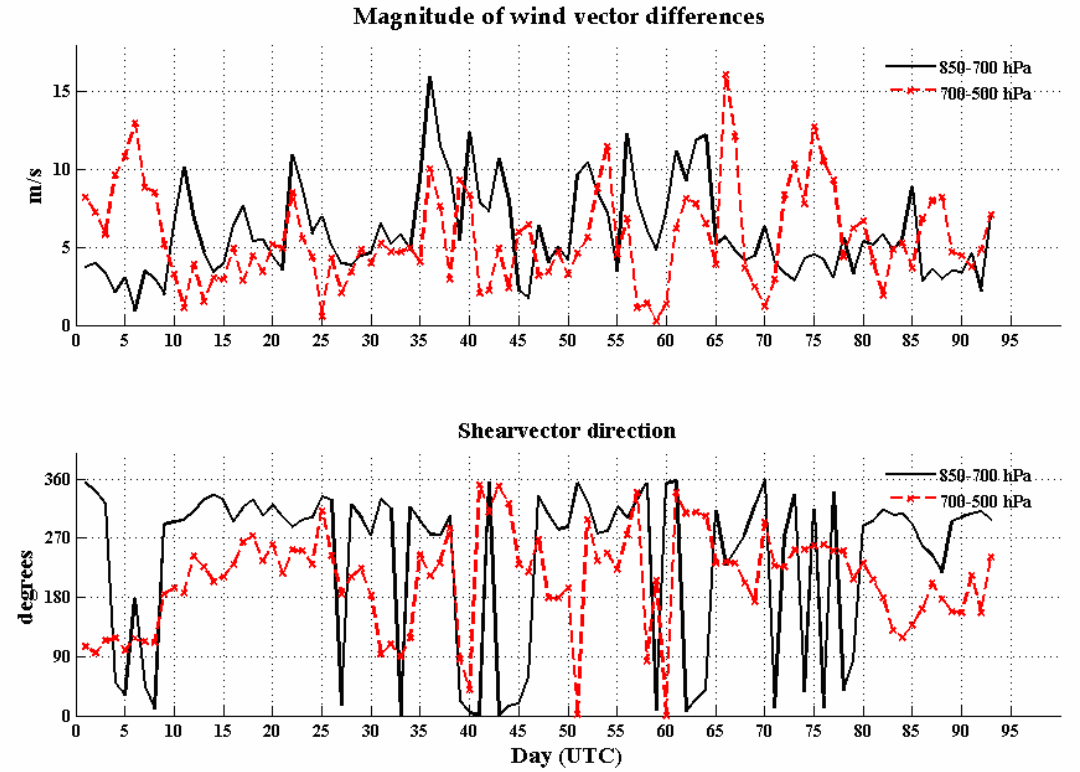

Figure 3-13. Wind vector differences in the 850-700 and 700-500 hPa layers, based on Darwin soundings from November 17, 2005 to February 17, 2006. The x-axis shows the day number (UTC day) starting with day 1 =17 November, 2005.

Table 3-2. Identification of shear regimes with the help of Darwin sounding data. Shear-perpendicular cases imply wind vector difference > 4 m s^{-1} in the 850-700 hPa layer, shear-parallel cases show a midlevel wind vector difference (> 5 m s^{-1}) that dominates over low level wind shear. The remaining one is defined for dates with strong opposite directed shear between low- and midlevels.

Type of convective line expected	Dates
Weak shear – no preferred type of line	20051129-20051130, 20051212-20051216, 20060103-20060105, 20060123-20060124, 20060126, 20060214-20060216
Low-level shear-perpendicular	20051117-20051119, 20051125-20051128, 20051208-20051212, 20051221-20051224, 20051226-20051230, 20060106-20060107, 20060111-20060119, 20060125, 20060209
Mid-level shear-parallel	20051117-20051124, 20060121-20060122, 20060127-20060201, 20060210-20060212
Midlevel shear opposite to low-level shear → 2D lines	20060127-20060201

The findings by LeMone et al. (1998) are graphically represented in figure 3-14 (left) together with frequencies of occurrence of orientations with respect to shear as a function of regime are shown in figure 3-14 (right). The contents of the graphs are

based on positive semi-definite records, i.e., the absolute value of angles. Therefore, we could expect cells to be biased away from the end points, i.e., away from 0^o and 90^o. The magnitude of this error depends on the uncertainty in orientations. However, the orientations of convective lines seem to agree with observations on radar loops and bar plots. Nevertheless, convective lines have been seen to be much more complicated than what would be anticipated from the idealisation in the left figure of fig. 3-14. Therefore, there is a contribution of noise in many of the observations. However, the number of records ranges from a bit more than 1000 up to about 10,000 for the different regimes, and the cell orientations can be treated as independent records. Therefore, any biases in the signals will have rather strong statistical significance.

3.5.1 Weak-shear conditions

Although shear was present also in this regime, it was the weakest found during the period of study, i.e., less than 5 m s^{-1} for both levels. Compared to the expected result by LeMone et al. (1998), the only strong signal found was that of the continental bias towards mid-level shear perpendicular orientations. This is a scenario not explained by LeMone et al. Since there is no preferred orientation with respect to low-level shear, it might be an indication of variable conditions, making it difficult to draw any conclusions. Radar loop studies showed complex behaviour of convective lines.

3.5.2 Expected low-level shear perpendicular cases

The results show that cells that occurred over land were generally near shear-perpendicular, similar to the TOGA-COARE results. This is likely a result of sea breeze effects since the low-level shear was mostly westerly during build-up and breaks, favouring convective lines oriented perpendicular to the shear with time. The peak in the distribution was at about 70^o. The aforementioned effect of values being biased away from the endpoints makes it reasonable to suspect that this signal is strong. One example is that of December 24 (see figure 3-10). However, the cell orientations over the ocean were found to be low-level-shear-*parallel*. This tendency might be explained in terms of decaying old convection moving offshore, and nocturnal convection from land-breezes favouring a zonal orientation of convective lines (see the subplots representing 12-18 and 18-24 UTC in figure 3-8). The nocturnal effect was confirmed by radar loop studies. This effect is mainly a feature of the build-up and break periods.

3.5.3 Expected mid-level shear parallel cases

These convective lines followed the expected results by LeMone et al. both over land and over the ocean. Cells were, in general, biased towards perpendicular orientations to the low-level shear and parallel to the mid-level shear. The mid-level shear parallel pattern is possibly because of the dominance of dry monsoon records.

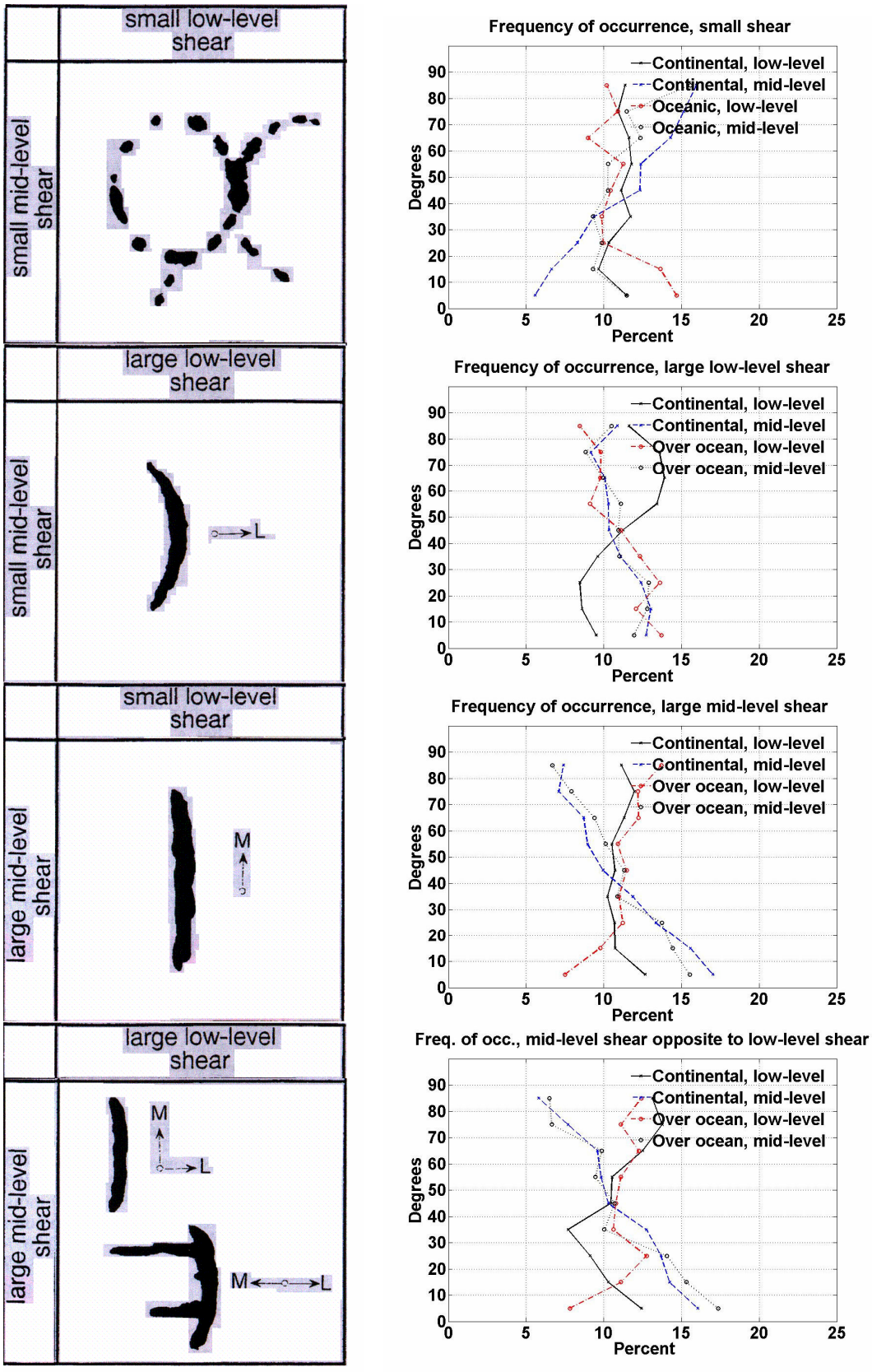

Figure 3-14. Left: Expected convective organisation in a homogeneous environment, given the indicated shear conditions at two levels (from LeMone et al., 1998). Right: Observed orientations with respect to shear at two levels separated into continental and oceanic records. The x-axis shows the percentage of all cells with a certain angle (see y-axis) with respect to shear. Based on TITAN data.

3.5.4 Expected 2D cases

The expectations might be confirmed over land, with a tendency towards low-level-shear-parallel *and* perpendicular orientations for continental records. This was not seen over the ocean, which showed a rather uniform distribution of orientations with respect to low-level shear. However, most of the cells were seen to be parallel to mid-level shear, which is indicative of the conditions during the dry monsoon, with a dominant mid-level shear.

3.5.5 Results

The study by LeMone at al. (1998) is based on conditions over the tropical western Pacific, and could therefore be hard to compare with the conditions around Darwin. Geographical features are seen to possibly play a major role in the organisation of convection, mostly in terms of sea breeze effects, but also in oceanic patterns with a possible nocturnal enhancement. The interaction between daytime organisation and night-time conditions is therefore suspected to be the primary driver of organising convective lines. It is anticipated that shear is the most important factor in the absence of large-scale geographically induced differences in important boundary layer properties. The convection seems to follow a diurnal pattern with low-level shear parallel orientations, evolving into shear-perpendicular structures during strong low-level shear conditions. This is in line with the findings of Keenan and Carbone (1992) and Wilson et al. (2000). The CAPPI loops also show periodic wave-like patterns at times, especially during the monsoon, reminiscent of fronts of enhanced convection moving in different directions super positioned on pre-existing convection. Radar loop studies have shown a high degree of complexity, and it is clear that many mechanisms are involved in organising the convection. It might well be so that individual cell orientations might not be as representative of convective line orientations as expected. This would act to mask some of the signals found through a strong noise. Further studies are needed to explore this relation.

3.6 Mergers and splits

It has been indicated that convective lines are regularly forming over both oceanic and continental regions of the radar coverage zone. The formation of a convective line is the process of merging cells into larger complexes. However, merging occurs also between cells not necessarily leading to the formation of convective lines. This section briefly describes the characteristics of mergers and splits in observed convection around Darwin, and TITAN has been used as a tool for separating mergers and splits from other cells in order to gain insight into differences between different cell types.

Complex cells tend to constitute about 25% of all cells occurring at any given hour of the day, but only roughly 15% of the cells for a specific day. This can be explained by

the observed longer lifetimes for complex cells, sometimes exceeding 3 hours whereas most isolated cells have lifetimes between 10 and 30 minutes. Mergers are found to be a dominating subset of complex cells, constituting almost 85% of all complex cells, whereas splits constitute the remaining fraction of the complex cells, i.e., ~15%. Therefore, mergers stand for roughly 12% and splits for a bit more than 2% of *all* cells that occur in the Darwin region on a daily basis. It was found that mergers occur in a wide variety of regimes whereas splits tend to be present during strong-wind regimes, making them a significant feature of the dry monsoon, during which they made up for more than 7% of the total number of cells. Many convective cells were then seen to split up as they were elongated into arc-shaped, near mid-level shear parallel formations along the convective lines. However, a majority of the mergers and splits were found in the beginning of the second monsoon onset, between January 12 and 14, when convection was widespread. Mergers were seen to persist once they formed, whereas splits usually were observed to dissipate earlier, since these often were the final phase of many systems, as seen in radar loops. Mergers were also seen to have more intense echoes confirming the results from earlier studies that mergers are based on more vigorous convection than other cells (Simpson et al., 1993; Westscott, 1994). The height distribution indicated that the echo cores of mergers reach higher altitudes, suggesting stronger updrafts and confirming observed higher reflectivities.

3.7 Statistical analysis

The preceding sections of this chapter have identified many features of the distributions of cell maximum heights, mean maximum reflectivity, cell speeds with respect to the 700 hPa flow and storm lifetimes. To draw any conclusions on observations, it is necessary to determine whether these are statistically significant or just a coincidence due to poor data. Some of the important observations will now be subject to statistical significance tests, which are common in atmospheric sciences and climatology in particular. Profiles of reflectivity will be introduced to support the observations of the first two variables, i.e., echo top heights and reflectivities.

3.7.1 Maximum height distribution and maximum reflectivities

The different regimes have been seen to support different vertical development of convective cores. Table D-1 in appendix D summarises some of the statistical observations, including the degree of statistical confidence. The subset of cells called non-squall-line cells are defined as all cells appearing in the radar zone not being part of the squall-line through its lifetime.

It is noteworthy that the vertical resolution of TITAN is 750 m. However, due to the large number of observations, in all cases exceeding 2340 records, with a minimum of 220 independent observations (storms), the results will be rather robust. The distribution of maximum height was found to follow a log-normal distribution fairly

well, similar to Cetrone and Houze (2006). In order to test the significance of observed differences between any two sets of data, a null hypothesis was considered for the lognormal distributions. The procedure of the test is outlined in appendix C. It is important to note that the discrete height values might influence the results, especially for cases with less data. However, to confirm the results, barplots and plots of the associated log-normal distributions were examined along with the tests. Also, the physical relevance is important. This is based on meteorological reasoning, i.e., if any observed differences leave enough to have significant meteorological impact, and if this reasoning is consistent with the results of the tests. The results are shown in table D-2, appendix D.

The vertical height distribution of 35 dBz echo tops is a good indicator of the magnitude of updrafts and intensity of storms. Also the maximum reflectivities of the cells under different regimes will aid to support the observations. The TITAN resolution for reflectivities is 0.5 dBz. The statistics are presented in table D-3, appendix D. Graphical representation of the max reflectivities shows that these are quasi-normally distributed, and therefore a t-test following the procedure in appendix C can be applied also here. The results follow in table D-4, appendix D.

It is not surprising that the build-up and breaks show higher vertical distribution of 35 dBz echo top heights than the monsoon. The build-up and breaks are showing robust signals in more intense convective cores than found during the monsoon, with a difference averaging 2 dBz. Therefore, it can be statistically confirmed that build-up and break storms are more intense than monsoon storms, supporting the study by Ballinger and May (2006). However, there is a weak tendency for cells occurring outside the Tiwi islands to be higher than those over the Tiwi islands during the build-up and breaks (Hectors). Despite this, Hectors are seen to have stronger return echoes. They are showing the same pattern when compared to squall-line cells in terms of intensities, but are similar in their vertical development. Hectors records are found at daytime during the build-up and breaks only, whereas some squall-lines occurred during the vertically less extensive monsoon regime and at night, so some overlap of samples is possible. Monsoon cells are clearly both more intense and vertically more developed than those during the dry monsoon.

Convective cores in mergers were seen to reach higher altitudes than the bulk of cells that occurred during the whole period of study, with a statistical confidence of more than 99% to reject the null hypothesis. This supports other studies, such as Westscott (1994) and Wilson et al. (2000). Mergers are also found to support more intense precipitation, as seen in the reflectivity distribution. Splits were seen to be statistically less vertically developed than other cells, which might be explained by the fact that these cells are often in a decaying phase with organisation breaking down. However, they do not show any significant differences from the bulk of cells in terms of mean max reflectivity. This suggests a sinking reflectivity core as seen in the lower max heights and neutral echo strength. The stronger forcing over the continent, as compared to that found over the ocean in terms of generating strong updrafts, is clear in the comparison between cells found over the ocean to those

found inland. Continental cells were vertically more extensive than those appearing over the ocean.

Shear is evidently an important parameter, since a strong low-level shear supports vertically higher cells than what a strong mid-level shear does. However, the intensities do not seem to differ between these two regimes. Since most of the cells under strong mid-level shear conditions occurred during the dry monsoon, it means that they were of oceanic origins, which was seen to support lower echo tops and was dominated by low mid-level humidity. The former is typical of oceanic convection (Keenan and Rutledge, 1993). This certainly acted to limit the heights rather than shear effects. Weak shear conditions are seen to be more favourable than any of the strong wind shear regimes. The weak wind regime was found mostly during build-up and breaks, but even when separating the strong shear regimes into build-up and breaks, the weak shear conditions still supported higher 35 dBz echo tops than any other shear regime.

3.7.2 Profiles of reflectivity

The studies of height distributions and the mean maximum reflectivities of cells have pinpointed some features of the differences in convective properties between different regimes. The profiles of cell reflectivity point towards some additional aspects of the vertical distribution and intensities. Figure 3-15 shows the median of the maximum reflectivities through the troposphere for the different regimes.

Build-up and breaks consistently show higher reflectivity values as compared to the monsoon throughout the troposphere. The suppressed dry monsoon shows the weakest profile with a rather quick drop in convective intensities through the depth of the troposphere, as compared to all other regimes.

The observed higher intensity for Hector cells vs. squall-line cells is distinct through all levels below 9 km, whereas Non-Hectors tend to dominate in the region between 6 and 9 km. The reasons for this observation is not clear. Mergers show more intense profiles than splits. The conclusion in the last section that the lower height distribution of split cells could be associated with dissipation of the cells is further supported by figure 3-15. It shows a consistently weaker profile compared to mergers. As expected, simple cells consistently show less intense return echoes than any of the two subsets mergers and splits.

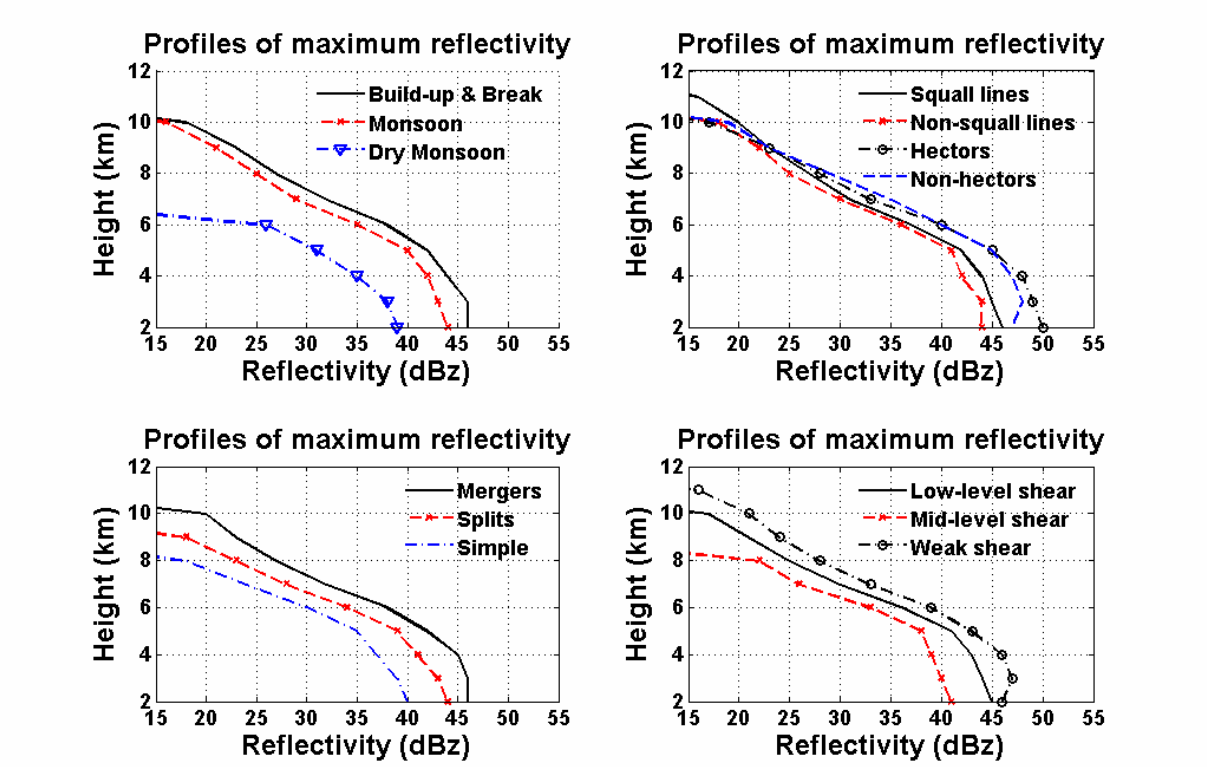

Figure 3-15. Profiles of median maximum reflectivities for the different regimes based on TITAN data. The profiles show the median reflectivity (dBz, x-axis) at certain heights (km, y-axis) separated into different regimes.

3.7.3 Cell speeds with respect to the 700 hPa wind

The speed of cells with respect to the "steering" flow at 700 hPa was studied because of its link to the dynamics (e.g. wind shear) of the cells as discussed in the section on squall-lines (3.2.2). Cells moving at least 3 ms^{-1} slower than the steering flow will be referred to as non-propagating, following Keenan and Carbone (1992). Those moving at least 3 ms^{-1} faster than the steering flow will accordingly be referred to as propagating cells. For intermediate values (=flow speed ± 3 ms^{-1}), cells are referred to as critical or balanced. Figure 3-16 demonstrates the frequency of occurrence of different cell speeds under various regimes. Only cells occurring on at least two subsequent TITAN tracks have been incorporated, since they are ascribed a zero-speed otherwise. Many differences between the regimes are manifested in the figure.

Build-up and break conditions tend to be dominated by cells that move slower than the 700 hPa easterly jet, whereas the monsoon and dry monsoon show a tendency towards more evenly distributed cell speeds, although a slight bias towards slower cell speeds can be seen. Daytime cells over the Tiwi islands (Hectors), as well as over the continent, are clearly non-propagating with respect to the 700 hPa wind on average, whereas squall-lines tend to be effectively steered by the 700 hPa wind. There are no clear internal distinctions in these two subsets of cells, although Hectors seem to be the slowest species of all in terms of propagation speed. Splits and mergers show similar behaviour, with splits slightly slower than mergers. Under

weak shear conditions, cells are seen to move slower than the 700 hPa wind. This is also evident for strong low-level shear regimes, whereas strong mid-level shear seem to favour balanced conditions because of the presence of a jet below 700 hPa.
Keenan and Carbone (1992) found that non-propagating cases in the Darwin region were favoured by high-shear conditions with a dominant easterly jet, whereas propagating cases were more likely to appear under weak mid-level wind regimes. The rearward tilt of the updraft under low-level jet regimes (e.g., the 700 hPa jet) favours the formation of a cold pool, which together with horizontal and vertical pressure gradients act to facilitate downward distribution of 700 hPa horizontal momentum. In extreme cases, when this momentum is largely unmixed, the cold pool can gain an additional 1-5 ms^{-1} to the spread-speed, helping the system to move with the speed of the low-level jet (Keenan and Carbone, 1992). The balanced state is essential for the longevity of squall-lines, which will be studied in next section.

Following the observations made above for figure 3-16 and seen in table D-5 in appendix D, cell speeds were tested statistically using a t-test, since they were seen to follow near normal distributions (see table D-6, appendix D).

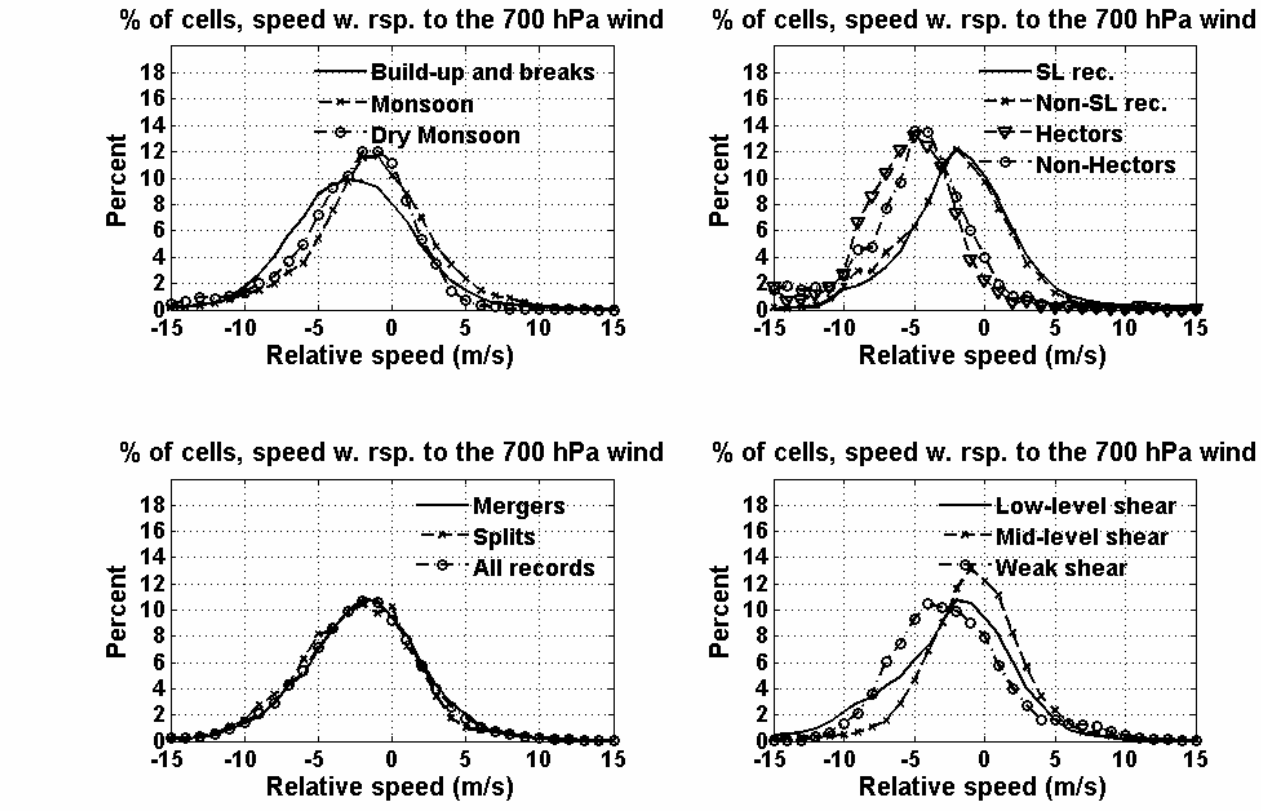

Figure 3-16. Cell speeds relative to the 700 hPa wind for different regimes. The x-axis shows the relative speed, whereas the y-axis shows the percentage of all cells that had the observed cell speed with respect to the 700 hPa wind speed. Based on TITAN data.

The results of the performed significance tests show that build-up and break storms move slower than monsoonal storms, which can be explained by the convective initiation mechanisms and the generally strong low-level shear. The presence of localised circulation phenomena such as sea breezes, acts to prevent a propagation

that is steered by the easterly jet during the build-up of convection during build-up and break periods. This is clear when looking at particularly Hectors, but also cells outside the Tiwi islands, which at daytime are slower (generally >5 ms^{-1} slower) than the easterly jet. These daytime extreme values are then regulated by propagating squall-lines and nocturnal convection, making up for the observed build-up and break values on the whole. The lower wind speed at midlevels during the monsoon possibly acts to increase the relative speed with respect to the 700 hPa wind of these systems. Squall-lines, monsoonal cells and cells occurring during strong midlevel shear regimes are seen to favour the most balanced cells, which might favour longer lifetimes for these cells.

3.7.4 Cell lifetimes

Following the discussion from the last section regarding the conditions that are favourable in sustaining convective cells, this section will look at the observed lifetimes of cells under different regimes. Shear is an important factor in many aspects of convective maintenance, such as dynamical organisation, cell speeds and initiation of other cells, following the development of cold pools. We therefore expect squall-lines, Hectors, monsoonal storms and mergers to be more persistent. Table D-7 in appendix D summarises some of the statistics regarding the duration of cells under different regimes. It is important to note the ten minutes difference between consecutive radar scans, which lowers the statistical significance. Records only appearing once have been excluded, and 5 minutes "extra lifetime" have been added to all cells to make up for the discrete nature of the records. Therefore, the important aspect is the difference between regimes rather than the absolute values.

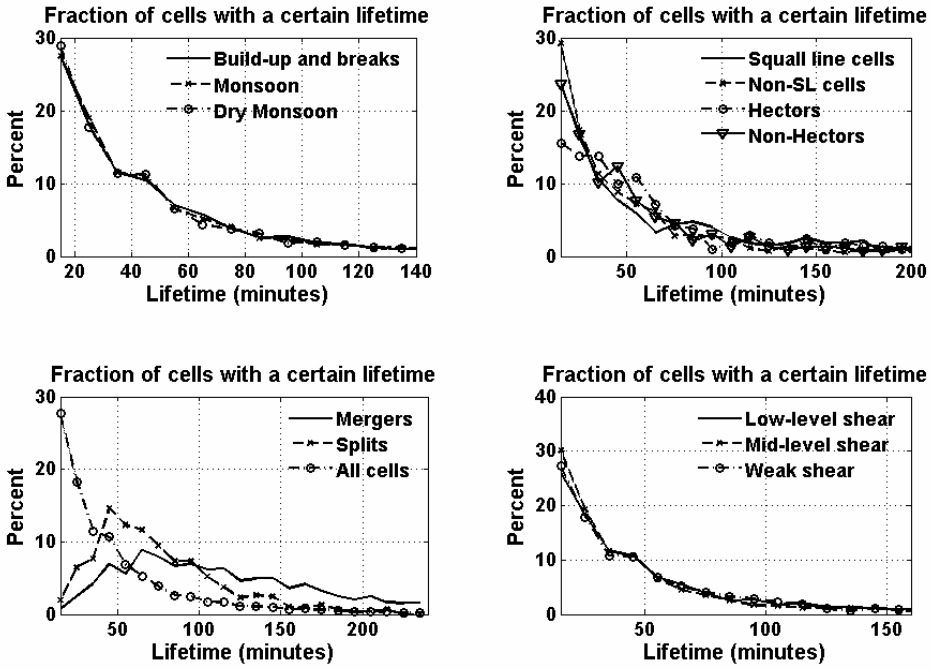

Figure 3-17. Probability distributions of cell lifetimes under various regimes based on TITAN records. The x-axis shows the lifetime in minutes, whereas the y-axis indicates the percentage of cells having a certain lifetime.

From table D-7 (appendix D) it can be seen that merged cells are the most long-lived ones, with a median lifetime of 105 minutes and a mean of 133 minutes. This is also the most prominent feature in figure 3-17. Also splits are seen to live longer than the bulk of other cells, which can be explained by the fact that these are consisting of more than one cell, whereas the bulk of cells are isolated. Squall-line cell lifetimes are longer than for Hectors and cells outside squall-lines, which is also in line with expectances from earlier discussion on sustainability. It is important to note that this is the lifetime of individual cells within the more long-lived squall-lines. There are no distinct differences between build-up and break storms vs. monsoon storms, which was found also by Ballinger and May (2006). The same is observed for strong low-level shear regimes vs. other shear regimes, with a slight tendency toward domination by strong low-level shear cells in terms of lifetime. This might be explained by the more favourable conditions for the build-up of squall-lines and Hectors during these conditions.

Chapter 4

Summary and conclusions

The convective characteristics of the Australian 2005/06 wet season in the Darwin region have been studied with the help of a storm identifying and tracking system (TITAN) based on radar retrievals. The wet season was subdivided into three different regimes; build-up/breaks, monsoon and dry monsoon. These were identified by the zonal component of a singe low level (700 hPa) wind and can be found in table 3-1. The dry monsoon was separated from the monsoon because of the presence of dry midlevel air due to a deep low in the interior of the Northern Territory. The separation into the different regimes showed that all were characterised by general upward motions, with a pronounced peak during the monsoon, consistent with other studies (e.g. Mapes and Houze, 1992; Keenan and Carbone, 1992; McBride and Frank, 1999; Ballinger and May, 2006).

The number of cells exceeding a 35 dBz threshold was seen to increase during monsoonal conditions. The equivalent potential temperatures were larger in the boundary layer during the build-up and breaks, as compared to other regimes. This reflects the observation that stronger forcing is needed to initiate convection during build-up and breaks, but when the conditional instability has been released, the high-θ_e air acts to feed the convective core with latent heat. The build-up and break periods were consequently showing a diurnal modulation of convection, whereas the monsoon and the dry monsoon had smaller diurnal cycles. The mean ascent of air during the monsoon induced widespread but less intense convection, typical of convection with oceanic origins (consistent with Keenan and Rutledge, 1993). This was seen in a larger area coverage of the cells, but a less common presence of cells exceeding the 45 dBz threshold.

The vertical development of cells during the different regimes was seen to follow a generally lognormal distribution, peaking around 7 km for the build-up/breaks and the monsoon. The presence of dry air at midlevels during the dry monsoon, and the lower θ_e at near-surface levels suppressed the vertical development of convection during this regime. Statistical significance tests were performed for the different regimes, showing that the convective cells of the build-up and breaks reached higher altitudes than any of the other regimes. The same was observed for the mean maximum reflectivities of the cells. The monsoon showed similar results compared to the dry monsoon, with the dry monsoon being the weaker subset.

The spatial distribution of cells showed different patterns for different regimes. This was indicative of the forcing mechanisms required to initiate convection. The build-up and breaks showed distinct peaks in frequency of occurrence that was confined to the Tiwi islands and near-coastal areas. Accordingly, sea breezes are suspected to be critical for the development of convection during these conditions, consistent with studies by, e.g., Keenan and Carbone (1992) and Wilson et al. (2000). The monsoon

showed a higher occurrence of more uniformly distributed convection in the western, i.e., oceanic sector, of the radar coverage zone. This indicates the oceanic origins of these cells, not dependent on the same forcing mechanisms. The dry monsoon showed different results, with convective lines that were semi-persistent, as was evident also in the spatial distribution for the period of 10 days. Hence, shear is suspected to be a major driver behind this observation, but further research is needed. The importance of shear as found in studies such as by LeMone et al. (1998) and Houze (1993), instigated an investigation of different shear regimes.

It was found that the build-up and breaks, which are dominated by an easterly jet at around the 700 hPa level, favoured early low-level shear parallel orientations over the continent and statistically significantly slower cell speeds than the steering flow. These cells initiated on sea breeze fronts and then evolved into low-level shear perpendicular orientations, which are more favourable for the convective maintenance (Houze, 1993; Keenan and Carbone, 1992). Often, the continental convective lines evolved into mature squall-lines, such as the case on December 24, 2005. The monsoon showed highly variable conditions in terms of shear due to the presence of synoptic scale disturbances, complicating the observed orientations with respect to shear and more complex interactions possibly including gravity waves.

The dry monsoon was characterised by a dominating mid-level shear, which was seen to favour mid-level shear parallel convective lines and cell orientations, with bursts of smaller scale meridional structures superimposed on these lines. This was possibly an indication of the dry midlevel air, facilitating the development of cold pools.

Strong low-level shear was found to favour the vertical development of cells but not necessarily the intensities compared to strong mid-level shear. This might reflect the dominance of squall-lines and Hectors during strong low-level shear conditions. However, weak shear dominated in terms of both vertical distribution and intensity. The reasons for this need to be further investigated.

Several other subsets of cells were studied, such as cells occurring over the Tiwi islands (i.e., Hectors), squall-line cells, mergers and splits, continental and over ocean cells. These were statistically compared through t-tests, as outlined in appendix C. Hectors were found to be more intense but vertically less extensive than corresponding continental cells. They were also found to live longer than cells outside the Tiwi islands. Continental records were seen to be vertically more extensive and have stronger return echoes, consistent with Keenan and Rutledge (1993).

Merging was seen to be a common feature throughout the period of study, making up for around 85% of all complex cells. Merged cells were by far the most intense subspecies in terms of echo top heights, reflectivity profiles and lifetimes similar to studies by, e.g., Westscott (1994). Splits, on the other hand, were found to be

shallower and shorter lived than other complex cells, indicating their likely appearance during the dissipating stage of convection.

For other regimes, the differences in terms of cell lifetimes were not as distinct, and the coarse temporal resolution of TITAN data makes it difficult to draw any conclusions on statistically significant differences.

The wet season showed a high degree of variability, and the Madden-Julian oscillation was a prominent feature at times, possibly affecting the onset and breaks of the monsoon. The period of study ended during the break, i.e., February 17. However, shortly after this date, a second onset of the monsoon was established, with associated larger decks of convection and substantial rainfall. Furthermore, a tropical cyclone formed over the Coral Sea and developed into a category 5 when reaching the Top End in the end of April 2006. For a complete study, also the period following February 17 should be incorporated, as well as more than only one season.

The study has shown the statistical behaviour in terms of vertical development, spatial occurrence, intensities and lifetimes of cells under different regimes. Given more time, many other aspects would be possible to study through the use of TITAN data. One implication of this study is that earlier case studies have been quantitatively assessed in terms of the convective behaviour under different regimes. Another implication is that the knowledge of the statistical behaviour of tropical convection in the Darwin region can be used to increase the accuracy in nowcasting and short-range forecasts. Not only are the findings applicable to the Darwin region, but they are also expected to be relevant to other monsoon regimes in the world. The findings can be a base for the parameterisation of convective storms in a wide range of models. A continuation of this study would include lower reflectivity thresholds to study also the cloud characteristics. With a polarimetric radar, microphysical classifications would be possible to integrate with the convective characteristics. This together with an integration of satellite data (e.g., TRMM) would considerably act to enhance the knowledge of convection in a tropical environment, and is a natural next step.

References

Alexandersson H., H. Bergström, 2005, Klimatologisk statistik med övningsuppgifter, Inst. för geovetenskaper, luft och vattenlära, Uppsala.

Andersson T., O. Persson, B. Lindström, 1985, Radarmeteorologi, Nr. 24, SMHI, Norrköping.

Ballinger A., P. T. May, 2005, The statistical characteristics of convective cell height, size and duration and their environmental characteristics in a monsoon regime (Darwin, Northern Australia), draft to be submitted to Journal of Climate.

Carbone R. E., T. D. Keenan, 1992, A preliminary morphology of precipitation systems in tropical northern Australia, Q. J. R. Meteorological Soc., **118**, 283.

Cetrone J., R. A. Houze Jr, 2006, Characteristics of Tropical Convection over the Ocean near Kwajalein, Monthly Weather Review, **134**, 834.

Dixon M., G. Wiener, 1993, TITAN: Thunderstorm Identification, Tracking, Analysis, and Nowcasting - A Radar-based Methodology, Journal of Atmospheric and Oceanic Technology, **10**, No. 6, 785.

Dixon M., 2005, TITAN Users' Guide, NCAR, Boulder Colorado.

Doviak R. J., D. S. Zrnic, 1993, Doppler Radar and Weather Observations, 2nd ed., Academic Press Inc., San Diego.

Drosdowsky W., 1996, Variability of the Australian summer monsoon at Darwin: 1957-1992, Journal of Climate, **9**, 85.

Halstead, H. J., 1965, Introduction to statistical methods, Griffin Press, Adelaide.

Hamilton K, R. A. Vincent, P. T. May, 2004, Darwin Area Wave Experiment (DAWEX) field campaign to study gravity wave generation and propagation, Journal of Geophysical Research, **109**.

Houze Jr R. A., B. Mapes, 1992, An integrated view of the 1987 Australian monsoon and its mesoscale convective systems, I: Horizontal structure, Q. J. R. Meteorological Soc., **118**, 927.

Houze R. A. Jr., 1993, Cloud dynamics, International Geophysics Series, **53**, Academic Press, San Diego.

Houze R. A. Jr, M. Steiner, 1997, Sensitivity of the Estimated Monthly Convective Rain Fraction to the Choice of Z-R Relation, Journal of Applied Meteorology, **36**, 452.

Johnson R. H., T. M. Rickenbach, S. A. Rutledge, P. E. Ciesielski, W. H. Schubert, 1999, Trimodal characteristics of tropical convection, Journal of Climate, vol. **12**, No 8, 2397.

Julian P. R., R. A. Madden, 1994, Observations of the 40-50-Day Tropical Oscillation – A Review, Montly Weather Review, **122**, 814.

Karlsson K.-G., 1997, Remote Sensing in Meteorology, 1st edition, Swedish Meteorological and Hydrological Institute, Norrköping.

Keenan T. D., S. A. Rutledge, 1993, Mesoscale Characteristics of Monsoonal Convection and Associated Stratiform Precipitation, Monthly Weather Review, **121**, No 2, 352.

LeMone M. A., E. J. Zipser, S. B. Trier, 1998, The Role of Environmental Shear and Thermodynamic Conditions in Determining the Structure and Evolution of Mesoscale Convective Systems during TOGA COARE, Journal of the Atmospheric Sciences, **55**, No 12, 3493.

May P. T., T. D. Keenan, 2005, Evaluation of Microphysical Retrievals from Polarimetric Radar with Wind Profiler Data, Journal of Applied Meteorology, **44**, 827.

May P. T., D. K. Rajopadhyaya, 1999, Vertical velocity characteristics of deep convection over Darwin, Australia, Monthly Weather Review, **127**, 1056.

McBride J. L. and W. M. Frank, 1999, Relationships between stability and monsoon convection, Journal of the Atmospheric Sciences, **56**, 24.

McBride J. L., M. C. Wheeler, W. K. M. Lau, D. E. Waliser, 2005, Intraseasonal variability in the atmosphere-ocean climate system, Springer-Praxis, Berlin-Heidelberg.

Moncrieff M. W., C. Liu, 1999, Convection Initiation by Density Currents: Role of Convergence, Shear and Dynamical Organization, Monthly Weather Review, **127**, No 10, 2455.

Ramage C. S., 1971, Monsoon Meteorology, International Geophysics Series, **15**, Academic Press, New York.

Riehl H., 1954, Tropical Meteorology, McGraw-Hill, London.

Rindert B., 1993, Termodynamik, hydrostatik och molnfysik, 2nd edition, Meteorologiska Institutionen, Uppsala Universitet.

Rogers R. R., M. K. Yau, 1989, A short course in cloud physics, 3rd edition, International Series in Natural Philosophy, **113**, Pergamon Press, Oxford.

Simpson J., T. D. Keenan, B. Ferrier, R. H. Simpson, G. J. Holland, 1993, Cumulus Mergers in the Maritime Continent Region, Meteorology and Atmospheric Physics, **51**, 73.

Sturman A., N. Tapper, 1996, The Weather and Climate of Australia and New Zealand, Oxford University Press, Melbourne.

Westscott N. E., 1994, Merging of Convective Clouds: Initiation, Bridging and Subsequent Growth, Monthly Weather Review, **122**, May, 780.

Wilks, D. S., 2006, Statistical methods in the Atmopsheric Sciences, 2nd edition, International Geophysics Series, **91**, Elsevier Inc., London.

Wilson J. W., R. E. Carbone, T. D. Keenan, J. M. Hacker, 2000, Tropical Island Convection in the Absence of Significant Topography. Part 1: Life Cycle of Diurnally Forced Convection, Monthly Weather Review, **128**, No 10, 3459.

Appendix A

A.1 Potential and equivalent potential temperatures

The potential temperature is the one an air parcel would adopt if it were moved from its present pressure level to the 1000 hPa level. It is given by:

$$\theta = T\left(\frac{1000}{p}\right)^{\eta_d}, \tag{A.1}$$

where T is the temperature (in K) of the air parcel, p is the pressure at which the air parcel is residing and η_d is given by

$$\eta_d = \frac{R_d}{c_{pd}}. \tag{A.2}$$

The index d is denoting dry air, R_d = 287.06 J kg^{-1} is the specific gas constant for dry air, and C_{pd} = 1004.71 J kg^{-1} is the specific heat capacity for dry air at a constant pressure. Accordingly, η_d = 0.2857.

The equivalent potential temperature is the one an air parcel would adopt if it were lifted dry adiabatically to the level of condensation, and then pseudo adiabatically lifted to the pressure level where all water vapour has condensed and left the air parcel, whereupon it is moved dry adiabatically to the 1000 hPa pressure level. It therefore gives an indication of both the temperature and the moisture content of the air parcel.

The equivalent potential temperature can be derived from the thermodynamic equation for moist air undergoing reversible processes (for a more thorough derivation and explanation of variables, the reader is referred to literature in thermodynamics):

$$(1+r)ds = \left[c_p + (r+r_l)c\right]\frac{dT}{T} - R_d\frac{dp_d}{p_d} + d\left(\frac{L_{wv}r}{T}\right). \tag{A.3}$$

Here r is the water vapour mixing ratio (mass of water vapour per mass of dry air), ds is the specific entropy, c_p as above, r_l the mass of liquid water per mass of dry air, T the temperature, p_d the partial pressure of dry air and L_{wv} the specific latent heat of water vapour. Assuming that the air parcel is an isolated system, it can be rewritten to the following form:

$$\left[c_p + (r+r_l)c\right]\frac{dT}{T} - R_d\frac{dp_d}{p_d} + d\left(\frac{L_{wv}r}{T}\right) = 0. \tag{A.4}$$

Furthermore, assuming $c_p + (r + r_l)c \approx c_p$ and making use of the fact that all differentials in (A.4) are exact differentials, we can integrate between two thermodynamic states without having to care about the path of integration.
Integration according to the process explained above and making use of (A.1) gives us the following relation for the conservative equivalent potential temperature:

$$\theta_e = \theta \cdot \exp\left(\frac{L_{wv} r_s}{c_{pd} T_s}\right). \tag{A.5}$$

L_{wv} is given empirically by:

$$L_{wv} = 2.5008 \cdot 10^6 - 2348.4 \cdot t, \tag{A.6}$$

where t is here the temperature in °C. In A.5, r_s is the mixing ratio at saturation for a given temperature and is given by:

$$r_s = \frac{\varepsilon \cdot e_s}{p - e_s}. \tag{A.7}$$

Here ε = 0.62198 is the ratio between the specific gas constant for dry air and water vapour, e_s is the water vapour pressure at saturation and p the total pressure. Furthermore, e_s is given by using, e.g., Bolton's empirical formula:

$$e_s = 6.1121 \cdot e^{\frac{17.67t}{243.5+t}}. \tag{A.8}$$

Here T_s is the condensation temperature and is given by the approximate formula:

$$T_s = \frac{6 \cdot T_d - T}{5}. \tag{A.9}$$

Here T_d is the dew point temperature given by:

$$T_d = \frac{T}{1 + \frac{R_d \cdot T}{\varepsilon \cdot l_{wv}} \ln\left(\frac{100}{r}\right)}. \tag{A.10}$$

Equation (A.1) to (A.10) have been used to derive the profiles of equivalent potential temperature in figure 2-2.

A.2 Pressure coordinates

Pressure coordinates can be used in atmospheric sciences to represent the vertical motion of air. The vertical speed (in Pa s^{-1}) is defined positive for descending motions (pressure increasing downward in the atmosphere):

$$\omega = \frac{dp}{dt}. \tag{A.11}$$

Using (A.11), (A.12) and the hydrostatic equation,

$$dp = -g\rho \cdot dz, \tag{A.12}$$

where dp is the pressure difference in a layer dz, g is the gravitational acceleration and ρ is the density at height z, gives:

$$\frac{dz}{dt} = -\frac{\omega}{g\rho}. \tag{A.13}$$

We approximate the environmental atmosphere to be close to the ICAO standard atmosphere and use the following relation:

$$\rho(z) = \rho_0 \left(1 - \frac{\gamma_v (z - z_0)}{T_{v0}} \right)^{\frac{g}{R_d \gamma_v} - 1}. \tag{A.14}$$

Here ρ_0 is the density at the base level, γ_v is the virtual temperature lapse rate, z is the height, T_{v0} is the virtual temperature at the base and all other parameters as in the preceding equations. The virtual temperature and its associated lapse rate are given by:

$$T_v = (1 + 0.61 \cdot q) \cdot T, \tag{A.15}$$

$$\gamma_v = -\frac{dT_v}{dz}. \tag{A.16}$$

Here q is the specific humidity as given by the mixing ratio:

$$q = \frac{r}{1 + r}. \tag{A.17}$$

Using (A-11) to (A-17) allows the transformation of vertical velocities in pressure coordinates to cartesian coordinates and metric values.

Appendix B

TITAN variables

The following parameters have been collected for each storm identified by TITAN as retrieved from radar scans. These data have then been used in the organisation of statistics throughout the study. It gives a sense of what kind of data that are possible to retrieve from the TITAN system. To create a matrix containing all these data, a set of program has been developed to handle this, and can be given on request.

1. Complex Track Number
2. Simple Track Number
3. Year
4. Month
5. Day
6. Hour
7. Minute
8. Second
9. x-coordinate of storm centre (km)
10. y-coordinate of storm centre (km)
11. Latitude (degrees)
12. Longitude (degrees)
13. Area of precipitation (km^2)
14. Precipitation rate (mm/hr)
15. Storm radius – major (km)
16. Storm radius – minor (km)
17. Storm orientation (degrees TN)
18. Volume of storm (km^3)
19. Mass of storm (x 10^6 kilograms)
20. Top of storm (km)
21. Maximum reflectivity (dBz)
22. Mean reflectivity (dBz)
23. Percentage of volume with reflectivity greater than 40 dBz
24. Percentage of volume with reflectivity greater than 50 dBz
25. Percentage of volume with reflectivity greater than 60 dBz
26. Percentage of volume with reflectivity greater than 70 dBz
27. Speed of storm movement (km/hr)
28. Direction of storm movement (degrees TN)
29. Rate of change of storm volume with time (km^3/hr)
30. Rate of change of storm area of precipitation with time (km^2/hour)
31. Vil (kg/m^2)
32. Height of maximum reflectivity (km)
33. x-coordinate of storm western boundary
34. x-coordinate of storm eastern boundary
35. y-coordinate of storm western boundary
36. y-coordinate of storm eastern boundary
37. Maximum reflectivity at height of 2 km (dBz)

    | ……
38. Maximum reflectivity at height of 19 km (dBz)

Appendix C

Statistical significance tests

In order to determine the statistical significance of some of the observations, the observations have been subject to statistical *t-tests*. These tests have been used to determine whether two data sets come from different distributions.
The logical procedure in the performance of these tests is given by Halstead (1965), Wilks (2006) and Alexandersson and Bergström (2005):

1. An assumption is made regarding the distribution that the data sets come from.
2. The hypothesis is that the data sets come from the same distribution.
3. Define an alternative hypothesis, e.g., the null hypothesis is not true.
4. Compare the samples and reject or accept the null hypothesis.

Most of the tested parameters, i.e., the 35 dBz echo max height, max reflectivity and speed with respect to 700 hPa wind, have been seen to approximately follow a normal distribution. In the case of the 35 dBz echo heights, these heights followed a log-normal distribution.

The frequency distribution of a variable in a normal distribution is given by

$$f(x) = \frac{1}{\sqrt{2\pi}\sigma}\exp\left(-\frac{(x-m)^2}{2\sigma^2}\right), \text{ x} \in \text{R}. \tag{C.1}$$

Here σ is the standard deviation and m is the expected value as derived from the mean of x. The associated cumulative distribution is given by

$$F(x) = \int_{-\infty}^{x'} \frac{1}{\sqrt{2\pi}\sigma}\exp\left(-\frac{(x'-m)^2}{2\sigma^2}\right)dx' . \tag{C.2}$$

This integral has no analytical solutions but can be simplified with the substitution $y = \frac{x'-m}{\sigma}$, giving equation (C.2) the following form:

$$F(x) = \int_{-\infty}^{\frac{x-m}{\sigma}} \frac{1}{\sqrt{2\pi}\sigma}\exp\left(-\frac{y^2}{2\sigma^2}\right)dy = \Phi\left(\frac{x-m}{\sigma}\right) \cong \Phi\left(\frac{\overline{x_0}-\overline{x}}{s/\sqrt{n}}\right). \tag{C.3}$$

Here Φ is the standardised normal distribution with a zero mean value and a standard deviation of 1, s is the standard deviation of an observation material with n observations, $\overline{x_0}$ is the mean value we wish to compare with to determine whether it is statistically different. The normal distribution can be found in statistical tables. The actual test use the following procedure, based on the observation that the difference between two normally distributed mean-values is normally distributed too:

$$t = \left| \frac{\overline{x_1} - \overline{x_2} - (m_1 - m_2)}{s_{\overline{x_1} - \overline{x_2}}} \right| \leq \alpha \,. \tag{C.4}$$

Here α determines the significance level we want to validate. As an example, α=1.96 gives a 95% confidence interval, and determines with what certainty the null hypothesis can be rejected. Using a null hypothesis we expect the m-values to be equal, and the equation above reduces accordingly. The larger the *t*, the larger the certainty. The mean values and standard deviations are given by:

$$\overline{x} = \frac{1}{n} \sum_{i=1}^{n} x_i \,, \tag{C.5}$$

$$s = \sqrt{\sum_{i=1}^{n} \frac{(x_i - \overline{x})^2}{n-1}} \,, \tag{C.6}$$

$$s_{\overline{x_1} - \overline{x_2}} = \sqrt{\frac{s_1^2}{n_1} + \frac{s_2^2}{n_2}} \,. \tag{C.7}$$

It is noteworthy that n_1 and n_2 need to be independent observations. For that reason, *n* is *not* always all *records* but rather the number of *storms* (independent entities). These numbers are given in the third column of the table below.

Table C-1. Number of records and storms for various regimes.

	Number of records	**Number of storms**
All cells	103503	11577
Build-up & Break	56862	5621
Monsoon	43494	4364
Dry Monsoon	3291	1613
Tiwi Isl. cells	2340	221
Outside Tiwi isl. cells	4853	637
Squall-line cells	14349	321
Non-squall-line cells	11510	1116
Over Ocean	52471	6193
Over Continent	66011	7410
Mergers	70585	2046
Splits	6119	628
Strong low-level shear	48434	4730
Strong mid-level shear	22964	3110
Weak shear	11573	1794

Appendix D

The results of statistical significance tests

This appendix summarises the observed statistics in terms of the outcome of statistical tests and statistical variables of importance, separated into the different regimes.

D.1 Height distribution

Table D-1. Height distribution statistics for different regimes based on TITAN tracks from Gunn Point, 35 dBz. Values are given in km except from the second column which shows the number of records.

	Number of rec.	Mean	Median	Standard Deviation	Lower quartile	Upper quartile	Min	Max
All cells	103503	7.1	6.6	2.1	5.9	8.1	1.4	20.1
Build-up & Breaks	56862	7.4	6.6	2.4	5.9	8.1	1.4	20.1
Monsoon	43494	6.7	6.6	1.6	5.9	7.4	2.1	17.1
Dry Monsoon	3291	5.8	5.9	1.1	5.1	6.6	3.6	10.4
Hectors	2340	7.4	6.6	2.6	5.9	8.1	2.9	18.6
Non-Hectors	4853	7.7	7.4	2.6	5.9	8.9	2.9	17.9
Squall-line cells	14349	7.3	6.6	2.4	5.9	8.1	1.4	18.6
Non-Squall-line cells	11510	7.0	6.6	2.1	5.9	7.4	2.1	18.6
Over ocean	52471	6.8	6.6	1.9	5.9	7.4	1.4	18.6
Continental	66011	7.0	6.6	2.2	5.9	7.4	2.1	20.1
Mergers	70585	7.4	6.6	2.3	5.9	8.1	1.4	20.1
Splits	6119	6.8	6.6	1.8	5.9	7.4	2.1	18.6
Strong low-level shear	48434	7.0	6.6	1.9	5.9	8.1	2.1	18.6
Strong mid-level shear	22964	6.7	6.6	1.9	5.9	7.4	2.1	19.4
Weak shear	11573	7.6	6.6	2.5	5.9	8.1	2.1	18.6

Table D-2. Results from t-tests approximated with a lognormal distribution and based on a null hypothesis.

	Dominant	t-value	Statistical significance	Physical significance	Confirmed by plot
Build-up & Breaks vs. Monsoon	Build-up & Breaks	15.6	>99%	Yes	Yes
Monsoon vs. Dry Monsoon	Monsoon	20.5	>99%	Yes	Yes
Hectors vs. Non-Hectors	Non-Hectors	1.9	90-95%	Not obvious	Yes
Hectors vs. squall-line cells	Hectors	0.6	<80%	Yes	Slightly
Squall-line vs. non-SL cells	Squall-line cells	1.5	80-90%	Yes	Not obvious

Mergers vs. all other cells	Mergers	5.7	>99%	Yes	Yes
Splits vs. all other cells	Other cells	3.6	>99%	Yes	Yes
Over ocean vs. continental cells	Continental	7.1	>99%	Yes	Yes
Strong low-level shear vs. strong mid-level shear cells	Low-level shear	7.2	>99%	Yes	Yes
Strong low-level vs. weak shear	Weak shear	9.2	>99%	No	Yes
Strong mid-level vs. weak shear	Weak shear	13.7	>99%	Not obvious	Yes

D.2 Maximum reflectivity

Table D-3. Distribution of reflectivities for different regimes based on TITAN tracks from Gunn Point, 35 dBz. Values are given in dBz, except from the second column showing the number of records.

	Number of records	**Mean**	**Median**	**Standard Deviation**	**Lower quartile**	**Upper quartile**
All cells	103503	48.9	49.0	5.8	44.5	53.0
Build-up & Breaks	56862	49.8	50.0	6.0	45.5	54.5
Monsoon	43494	47.8	48.0	5.3	44.0	51.5
Dry Monsoon	3291	47.4	47.0	4.1	44.5	50.0
Hectors	2340	52.4	53.0	5.4	48.5	56.5
Non-Hectors	4853	50.9	51.0	5.3	47.0	55.0
Squall-line cells	14349	48.8	49.0	6.2	44.0	53.5
Non-Squall-line cells	11510	48.1	48.0	5.9	43.5	52.5
Over ocean	52471	48.6	48.5	5.7	44.5	52.5
Continental	66011	48.7	48.5	5.7	44.5	53.0
Mergers	70585	49.4	49.5	5.9	45.0	53.5
Splits	6119	48.9	49.0	6.0	44.5	53.5
Strong low-level shear	48434	48.7	48.5	5.4	44.5	52.5
Strong mid-level shear	22964	48.8	49.0	5.9	44.5	53.0
Weak shear	11573	49.8	50.0	6.0	45.0	54.5

Table D-4. Results from t-tests on maximum reflectivities using a normal standard distribution and assuming a null hypothesis.

	Dominant	**t-value**	**Statistical significance**	**Physical significance**	**Confirmed by plot**
Build-up & Breaks vs. Monsoon	Build-up & Break	16.5	>99%	Yes	Yes
Monsoon vs. Dry Monsoon	Monsoon	3.0	>99%	Yes	Yes
Hectors vs. Non-Hectors	Hectors	3.4	>99%	Not obvious	Yes

Hectors vs. squall-line cells	Hectors	7.6	>99%	Not obvious	Yes
Squall-line vs. non-SL cells	Squall-line cells	1.7	90-95%	Yes	Yes
Mergers vs. all other cells	Mergers	3.8	>99%	Yes	Yes
Splits vs. all other cells	Neither	<0.1	<80%	Yes	Yes
Over ocean vs. continental cells	Continental	1.7	90-95%	Yes	Yes
Strong low-level shear vs. strong mid-level shear cells	Shear parallel	1.0	<80%	Not obvious	Yes
Strong low-level vs. weak shear	Weak shear	7.5	>99%	Not obvious	Yes
Strong mid-level vs. weak shear	Weak shear	5.8	>99%	Not obvious	Yes

D.3 Cell speeds with respect to the 700 hPa wind

Table D-5. Statistical summary of relative speed characteristics for various regimes. Values are in ms^{-1}, except from the second column showing the number of records.

	Number of records	**Mean**	**Median**	**Lower Quartile**	**Upper Quartile**	**Standard deviation of mean**
All cells	92346	-2.0	-2.0	-4.6	0.6	<0.1
Build-up & Break	44216	-2.6	-2.7	-5.4	0.0	0.1
Monsoon	38789	-1.2	-1.3	-3.6	1.2	0.1
Dry Monsoon	9447	-2.8	-2.1	-4.7	-0.0	0.1
Tiwi Isl. cells	1893	-5.7	-5.4	-7.7	-3.3	0.3
Outside Tiwi isl. cells	3745	-5.2	-4.7	-7.1	-2.6	0.2
Squall-line cells	12124	-1.7	-1.7	-4.0	0.7	0.2
Non-squall-line cells	8965	-2.2	-2.0	-4.5	0.3	0.1
Over Ocean	40970	-2.0	-1.9	-4.7	0.7	0.1
Over Continent	51943	-2.1	-2.0	-4.5	0.4	<0.1
Mergers	60813	-1.9	-1.9	-4.4	0.7	0.1
Splits	5509	-2.4	-2.2	-5.0	0.2	0.2
Strong low-level shear	38910	-2.4	-2.0	-5.0	0.5	0.1
Strong mid-level shear	22296	-0.8	-0.7	-2.9	1.3	0.1
Weak shear	14700	-2.2	-2.6	-5.1	0.0	0.1

Table D-6. Results of significance tests on cell speeds with respect to the 700 hPa wind between different regimes as determined by the left column.

	Least balanced	**t-value**	**Statistical significance**	**Confirmed by plot**
Build-up & Breaks vs. Monsoon	Build-up & Breaks	15.5	>99%	Yes
Build-up/Breaks vs. Dry Monsoon	Dry Monsoon	1.3	<90%	Not clear
Monsoon vs. Dry Monsoon	Dry Monsoon	12.6	>99%	Yes

Hectors vs. Non-Hectors	Hectors	1.4	80-90%	Not clear
Hectors vs. squall-line cells	Hectors	11.0	>99%	Yes
Squall-line vs. non-SL cells	Non-SL cells	1.91	90-95%	Yes
Mergers vs. all other cells	Mergers	1.1	<80%	Not clear
Splits vs. all other cells	Splits	2.1	>95%	Yes
Over ocean vs. continental cells	Continental	1.0	<80%	Not clear
Strong low-level shear vs. strong mid-level shear cells	Strong lowlevel shear cells	15.0	>99%	Yes
Strong low-level vs. weak shear	----- || ----------	1.9	90-95%	Yes
Strong mid-level vs. weak shear	Weak shear cells	11.2	>99%	Yes

D.4 Cell Lifetimes

Table D-7. Summarising statistics, cell lifetimes under various regimes. Based on TITAN tracks. Values are in minutes, except from the second column showing number of cells.

	Number of cells	**Median**	**Lower Quartile**	**Upper Quartile**	**Mean**	**Standard deviation of mean**
All cells	11577	35	15	65	53	1
Build-up & Break	5621	35	15	65	54	1
Monsoon	4364	35	15	65	54	1
Dry Monsoon	1613	35	15	55	49	1
Tiwi Isl. cells	221	45	25	75	74	5
Outside Tiwi isl. cells	637	45	25	75	64	3
Squall-line cells	321	55	25	135	112	8
Non-squall-line cells	1116	35	15	65	55	2
Over Ocean	6193	35	25	75	62	1
Over Continent	7410	35	25	75	61	1
Mergers	2046	105	65	165	133	2
Splits	628	65	45	95	74	2
Strong low-level shear	4730	35	15	65	55	1
Strong mid-level shear	3110	35	15	55	50	1
Weak shear	1794	35	15	65	55	1

Tidigare utgivna publikationer i serien ISSN 1650-6553

Nr 1 **Geomorphological mapping and hazard assessment of alpine areas in Vorarlberg, Austria**, Marcus Gustavsson

Nr 2 **Verification of the Turbulence Index used at SMHI**, Stefan Bergman

Nr 3 **Forecasting the next day's maximum and minimum temperature in Vancouver, Canada by using artificial neural network models**, Magnus Nilsson

Nr 4 **The tectonic history of the Skyttorp-Vattholma fault zone, south-central Sweden**, Anna Victoria Engström

Nr 5 **Investigation on Surface energy fluxes and their relationship to synoptic weather patterns on Storglaciären, northern Sweden**, Yvonne Kramer

Nr 6 **Förekomst och utlakning av bly från Tudors industriområde i Nol**, Anna Bohlin

Nr 7 **Partial Melting in Granulite Gneisses from Hornslandet, SE Central Sweden**, Sofia Carlsson

Nr 8 **Högupplösande processering av seismiska data insamlade nära Gardermoens flygplats**, Marie Larsson

Nr 9 **Sedimentundersökning i Lillsjön och Vikern Gyttorp**, Jan Sävås

Nr 10 **Integrering av MIFO och Grundvattenmodeller**, Marit Brandt

Nr 11 **GIS-baserad förstudie till MKB för behandling av förorenade jordmassor i Stockholms respektive Södermanlands län**, Borka Medjed-Hedlund

Nr 12 **Groundwater Chemistry in the Area East of the Dead Sea, Jordan**, Alice Nassar

Nr 13 **Bly i morän och vatten i delar av Småland, naturligt eller antropogent?**, Karin Luthbom

Nr 14 **Metanflöde mellan väldränerad, subarktisk tundra och atmosfären -betydelsen av markens vattenhalt och kemiska egenskaper**, Gunilla Nordenmark

Nr 15 **Effects of isothermal versus fluctuating temperature regimes on CO_2 efflux from sub-arctic soils**, Pär Eriksson

Nr 16 **En dagvattenmodell för beräkning av avrinning och transport av kväve och fosfor i Flatendiket i södra Stockholm**, Sara-Sofia Hellström

Nr 17 **Långsiktiga effekter av odlingsinriktning på förändringar i markens humusförråd - en fallstudie,** Helena Näslund

Nr 18 **Dynutveckling längs kusten utanför Halmstad, under senare hälften av 1900-talet.** Ingrid Engvall

Nr 19 **Humidity Structures in the Marine Atmospheric Boundary Layer,** Andreas Svensson

Nr 20 **The Influence of Waves on the Heat Exchange over Sea,** Erik Sahlée

Nr 21 **Åska längs Sveriges kuster,** Ulrika Andersson

Nr 22 **En enkel modell för beräkning av tjäldjup,** Johan Hansson

Nr 23 **Modelling the Wind Climate in Mountain Valleys Using the MIUU Mesoscale Model,** Nikolaus Juuso

Nr 24 **Evaluation of a New Lateral Boundary Condition in the MIUU Meso-Scale Model,** Anna Jansson

Nr 25 **Statistisk studie av sambandet mellan geostrofisk vind och temperatur i södra Sverige,** Jonas Höglund

Nr 26 **A comparison of the temperature climate at two urban sites in Uppsala,** Paulina Larsson

Nr 27 **Optiska djupet för atmosfäriska aerosolpartiklar över södra Sverige,** Jonas Lilja

Nr 28 **The wind field in coastal areas,** Niklas Sondell

Nr 29 **A Receiver Function Analysis of the Swedish Crust,** David Mawdsley

Nr 30 **Tjäldjupsberäkningar med temperatursummor,** Malin Knutsson

Nr 31 **Processing and Interpretation of Line 4 Seismic Reflection Data from Siljan Ring Area,** Daniela Justiniano Romero

Nr 32 **Turning Ray Tomography along deep Reflection Seismic Line 4 from the Siljan Ring Area,** Anmar C. Dávila Chacón

Nr 33 **Comparison of two small catchments in the Nopex research area by water balance and modelling approaches,** Ulrike Kummer

Nr 34 **High resolution data processing of EnviroMT data,** Tobias Donner

Nr 35 **Paleoclimatic conditions during late Triassic to early Jurassic, northern North Sea: evidence from clay mineralogy,** Victoria Adestål

Nr 36 **Controlled Source Magnetotellurics - The transition from near-field to far-field** Hermann Walch

Nr 37 **Soil respiration in sub-arctic soils – controlling factors and influence of global change,** Evelina Selander

Nr 38 **Miljöeffekter av Triorganiska tennföreningar från antifoulingfärg – med avseende på sedimentologi, ekotoxikologi och hydrogeologi**, Sara Berglund

Nr 39 **Depth distribution of methanotroph activity at a mountain birch forest-tundra ecotone, northern Sweden,** Erik Melander

Nr 40 **Methyl tert-Butyl Ether Contamination in Groundwater,** Linda Ahlström

Nr 41 **Geokemisk undersökning av vattnet i Västerhavet Med avseende på metallhalter och ^{129}I,** Anette Bergström

Nr 42 **Fracture filling minerals and the extent of associated alteration into adjacent granitic host rock,** Erik Ogenhall

Nr 43 **Bi-Se minerals from the Falun Copper mine,** Helena Karlsson

Nr 44 **Structures and Metamorphism in the Heidal-Glittertindarea, Scandinavian Caledonides,** Erik Malmqvist

Nr 45 **Structure and isotope-age studies in Faddey Bay region of central Taymyr, northern Siberia,** Robert Eriksson

Nr 46 **Stabilitetsindex – en stabil prognosmetod för åska?,** Johan Sohlberg

Nr 47 **Stadsklimateffekter i Uppsala,** Andreas Karelid

Nr 48 **Snow or rain? - A matter of wet-bulb temperature,** Arvid Olsen

Nr 49 **Beräkning av turbulenta flöden enligt inertial dissipationsmetoden med mätdata från en specialkonstruerad lättviktsanemometer samt jämförelse med turbulenta utbytesmetoden,** Charlotta Nilsson

Nr 50 **Inverkan av det interna gränsskiktets höjd på turbulensstrukturen i ytskiktet,** Ulrika Hansson

Nr 51 **Evaluation of the Inertial Dissipation Method over Land,** Björn Carlsson

Nr 52 **Lower Ordovician Acritarchs from Jilin Province, Northeast China,** Sebastian Willman

Nr 53 **Methods for Estimating the Wind Climate Using the MIUU-model,** Magnus Lindholm

Nr 54 **Mineralogical Evolution of Kaolinite Coated Blast Furnace Pellets,** Kristine Zarins

Nr 55 **Crooked line first arrival refraction tomography near the Archean-Proterozoic in Northern Sweden,** Valentina Villoria

Nr 56 **Processing and AVO Analyses of Marine Reflection Seismic Data from Vestfjorden, Norway,** Octavio García Moreno

Nr 57 **Pre-stack migration of seismic data from the IBERSEIS seismic profile to image the upper crust,** Carlos Eduardo Jiménez Valencia

Nr 58 **Spatial and Temporal Distribution of Diagenetic Alterations in the Grés de la Créche Formation (Upper Jurassic, N France),** Stefan Eklund

Nr 59 **Tektoniskt kontrollerade mineraliseringar i Oldenfönstret, Jämtlands län,** Gunnar Rauséus

Nr 60 **Neoproterozoic Radiation of Acritarchs and Environmental Perturbations around the Acraman Impact in Southern Australia,** Mikael Axelsson

Nr 61 **Chlorite weathering kinetics as a function of pH and grain size,** Magdalena Lerczak and Karol Bajer

Nr 62 **H_2S Production and Sulphur Isotope Fractionation in Column Experiments with Sulphate - Reducing Bacteria,** Stephan Wagner

Nr 63 **Magnetotelluric Measurements in the Swedish Caledonides,** Maria Jansdotter Carlsäter

Nr 64 **Identification of Potential Miombo Woodlands by Remote Sensing Analysis,** Ann Thorén

Nr 65 **Modeling Phosphorus Transport and Retention in River Networks,** Jörgen Rosberg

Nr 66 **The Importance of Gravity for Integrated Geophysical Studies of Aquifers,** Johan Jönberger

Nr 67 **Studying the effect of climate change on the design of water supply reservoir,** Gitte Berglöv

Nr 68 **Source identification of nitrate in a Tertiary aquifer, western Spain: a stable-isotope approach,** Anna Kjellin

Nr 69 **Kartläggning av bly vid Hagelgruvan, Gyttorp,** Ida Florberger

Nr 70 **Morphometry and environmental controls of solifluction landforms in the Abisko area, northern Sweden,** Hanna Ridefelt

Nr 71 **Trilobite biostratigraphy of the Tremadoc Bjørkåsholmen Formation on Öland, Sweden,** Åsa Frisk

Nr 72 **Skyddsområden för grundvattentäkter - granskning av hur de upprättats,** Jill Fernqvist

Nr 73 **Ultramafic diatremes in middle Sweden,** Johan Sjöberg

Nr 74 **The effect of tannery waste on soil and groundwater in Erode district, Tamil Nadu, India** *A Minor Field Study,* Janette Jönsson

Nr 75 **Impact of copper- and zinc contamination in groundwater and soil, Coimbatore urban areas, Tamil Nadu, South India** *A Minor Field Study,* Sofia Gröhn

Nr 76 **Klassificering av Low Level Jets och analys av den termiska vinden över Östergarnsholm** , Lisa Frost

Nr 77 **En ny metod för att beräkna impuls- och värmeflöden vid stabila förhållanden**, Anna Belking

Nr 78 **Low-level jets - observationer från Näsudden på Gotland**, Petra Johansson

Nr 79 **Sprite observations over France in relation to their parent thunderstorm system**, Lars Knutsson

Nr 80 **Influence of fog on stratification and turbulent fluxes over the ocean**, Linda Lennartsson

Nr 81 **Statistisk undersökning av prognosmetod för stratus efter snöfall**, Elisabeth Grunditz

Nr 82 **An investigation of the surface fluxes and other parameters in the regional climate model RCA1during ice conditions**, Camilla Tisell

Nr 83 **An investigation of the accuracy and long term trends of ERA-40 over the Baltic Sea**, Gabriella Nilsson

Nr 84 **Sensitivity of conceptual hydrological models to precipitation data errors – a regional study**, Liselotte Tunemar

Nr 85 **Spatial and temporal distribution of diagenetic modifications in Upper Paleocene deep-water marine, turbiditic sandstones of the Faeroe/Shetland basin of the North Sea**, Marcos Axelsson

Nr 86 **Crooked line first arrival refraction tomography in the Skellefte ore field, Northern Sweden**, Enrique Pedraza

Nr 87 **Tektoniken som skulptör - en strukturgeologisk tolkning av Stockholmsområdet och dess skärgård,** Peter Dahlin

Nr 88 **Predicting the fate of fertilisers and pesticides applied to a golf course in central Sweden, using a GIS Tool,** Cecilia Reinestam

Nr 89 **Formation of Potassium Slag in Blast Furnace Pellets**, Elin Eliasson

Nr 90 **- Syns den globala uppvärmningen i den svenska snöstatistiken?**Mattias Larsson

Nr 91 **Acid neutralization reactions in mine tailings from Kristineberg**, Michal Petlicki och Ewa Teklinska

Nr 92 **Ravinbildning i Naris ekologiska reservat, Costa Rica**, Axel Lauridsen Vang

Nr 93 **Temporal variations in surface velocity and elevation of Nordenskiöldbreen, Svalbard**, Ann-Marie Berggren

Nr 94 **Beskrivning av naturgeografin i tre av Uppsala läns naturreservat**, Emelie Nilsson

Nr 95 **Water resources and water management in Mauritius,** Per Berg

Nr 96 **Past and future of Nordenskiöldbreen, Svalbard,** Peter Kuipers Munneke

Nr 97 **Micropaleontology of the Upper Bajocian *Ostrea acuminata* marls of Champfromier (Ain, France) and paleoenvironmental implications,** Petrus Lindh

Nr 98 **Calymenid trilobites (Arthropoda) from the Silurian of Gotland**, Lena Söderkvist

Nr 99 **Development and validation of a new mass-consistent model using terrain-influenced coordinates,** Linus Magnusson

Nr 100 **The Formation of Stratus in Rain,** Wiebke Frey

Nr 101 **Estimation of gusty winds in RCA,** Maria Nordström

Nr 102 **Vädermärken och andra påståenden om vädret - sant eller falskt?,** Erica Thiderström

Nr 103 **A comparison between Sharp Boundary inversion and Reduced Basis OCCAM inversion for a 2-D RMT+CSTMT survey at Skediga, Sweden,** Adriana Berbesi

Nr 104 **Space and time evolution of crustal stress in the South Iceland Seismic Zone using microearthquake focal mechanics,** Mimmi Arvidsson

Nr 105 **Carbon dioxide in the atmosphere: A study of mean levels and air-sea fluxes over the Baltic Sea,** Cristoffer Wittskog

Nr 106 **Polarized Raman Spectroscopy on Minerals,** María Ángeles Benito Saz

Nr 107 **Faunal changes across the Ordovician – Silurian boundary beds, Osmundsberget Quarry, Siljan District, Dalarna,** Cecilia Larsson

Nr 108 **Shrews (Soricidae: Mammalia) from the Pliocene of Hambach, NW Germany,** Sandra Pettersson

Nr 109 **Waveform Tomography in Small Scale Near Surface Investigations,** Joseph Doetsch

Nr 110 **Vegetation Classification and Mapping of Glacial Erosional and Depositional Features** ***Northeastern part of Isla Santa Inés, 53^{0}S and 72^{0}W, Chile,*** Jenny Ampiala

Nr 111 **Recent berm ridge development inside a mesotidal estuary** ***The Guadalquivir River mouth case,*** Ulrika Åberg

Nr 112 **Metodutveckling för extrahering av jod ur fasta material,** Staffan Petré

Nr 113 **Släntstabilitet längs Ångermanälvens dalgång,** Mia Eriksson

Nr 114 **Validation of remote sensing snow cover analysis,** Anna Geidne

Nr 115 **The Silver Mineralogy of the Garpenberg Volcanogenic Sulphide Deposit, Bergslagen, Central Sweden,** Camilla Berggren

Nr 116 **Satellite interferometry (InSAR) as a tool for detection of strain along End-Glacial faults in Sweden,** Anders Högrelius

Nr 117 **Landscape Evolution in the Po-Delta, Italy,** Frida Andersson

Nr 118 **Metamorphism in the Hornslandet Area, South - East Central Sweden,** Karl-Johan Mattsson

Nr 119 **Contaminated Land database** - GIS as a tool for Contaminated Land Investigations**,** Robert Elfving

Nr 120 **Geofysik vid miljöteknisk markundersökning,** Andreas Leander

Nr 121 **Precipitation of Metal Ions in a Reactive Barrier with the Help of Sulphate - Reducing Bacteria,** Andreas Karlhager

Nr 122 **Sensitivity Analysis of the Mesoscale Air Pollution Model TAPM,** David Hirdman

Nr 123 **Effects of Upwelling Events on the Atmosphere,** Susanna Hagelin

Nr 124 **The Accuracy of the Wind Stress over Ocean of the Rossby Centre Atmospheric Model (RCA),** Alexandra Ohlsson